

# Two-point correlators in de Sitter-prepared states with bra-ket wormholes

---

Sunghoon Jung,<sup>a,b</sup> Minju Kum,<sup>c,a</sup> Junghwan Lee<sup>a</sup>

<sup>a</sup>*Center for Theoretical Physics, Department of Physics and Astronomy,  
Seoul National University, Seoul 08826, Korea*

<sup>b</sup>*Astronomy Research Center, Seoul National University, Seoul 08826, Korea*

<sup>c</sup>*Department of Physics, University of Texas at Austin, Austin, TX 78712, USA*

*E-mail:* [sunghoonj@snu.ac.kr](mailto:sunghoonj@snu.ac.kr), [minjukum@utexas.edu](mailto:minjukum@utexas.edu), [ghe1266@snu.ac.kr](mailto:ghe1266@snu.ac.kr)

**ABSTRACT:** Motivated by the finiteness of de Sitter (dS) horizon entropy, we study how “bra-ket wormholes” modify correlation functions in gravitationally prepared states. Euclidean wormhole saddles in gravitational path integrals can generate non-factorizing contributions to correlation functions, as in replica-wormhole explanation of the Page curve and bra-ket-wormhole restoration of strong subadditivity. By defining ‘time’ variables and computing observables in a flat region attached to the dS boundary, we evaluate bra-ket wormhole contributions to scalar two-point functions and find a late-time transition in the dominant saddle, accompanied by ramp-and-plateau behavior of correlations and a characteristic timescale comparable to the fast scrambling. Our results are built upon (i) inflationary horizon exit and re-entry, (ii) enhancement of correlation at small comoving momentum  $k$  by wormhole contribution, and (iii) a competition between mode counting and topological suppression that drives a transition to wormhole dominance. Although results are qualitatively consistent, one needs to address wormhole stabilization to clearly interpret in terms of the entropy context.

---

## Contents

<b>1</b>	<b>Introduction</b>	<b>1</b>
<b>2</b>	<b>Gravitationally prepared state at the end of inflation</b>	<b>3</b>
2.1	Gravitational state preparation, and consistency	4
2.2	Observation of dS prepared state, notion of time	6
<b>3</b>	<b>Wormholes for two-point correlations of scalar QFT</b>	<b>7</b>
3.1	Equations of motion and boundary conditions in the global coordinate	7
3.2	Naive bra-ket wormholes do not exist at NLO	9
3.3	Bra-ket wormhole by tracing out unobservable universe	12
3.4	Stabilization of wormholes	13
<b>4</b>	<b>Observables of bra-ket wormholes</b>	<b>15</b>
4.1	Notions of time: $k_{\max}$ and $k_{\min}$	15
4.2	Phase transition to wormhole dominance	16
4.3	Observable 1 - Comparing longer and shorter inflation	17
4.4	Observable 2 - CMB-like correlation after reheating	20
<b>5</b>	<b>Summary and Discussion</b>	<b>21</b>
<b>A</b>	<b>Scalar field solutions and correlators</b>	<b>25</b>
A.1	Hartle-Hawking	25
A.2	Two-boundary wormhole	27
<b>B</b>	<b>Stabilizing bra-ket wormhole by extra fermions</b>	<b>28</b>
<b>C</b>	<b><math>\tau_0</math> dependence</b>	<b>30</b>
<b>D</b>	<b>Suppression of contributions from multiple wormholes</b>	<b>30</b>

---

## 1 Introduction

De Sitter(dS) spacetime possesses a cosmological horizon with Gibbons–Hawking thermodynamics [1], associated with a finite entropy given by the Bekenstein-Hawking area law [2, 3]

$$S_{\text{dS}} \sim \frac{A_{\text{h}}}{4G\hbar}, \quad (1.1)$$

and—at least for suitably defined observables—a finite effective Hilbert space dimension,

$$\dim \mathcal{H} \sim e^{S_{\text{dS}}}. \quad (1.2)$$

If this interpretation is correct, then dS quantum gravity should exhibit the characteristic long-time constraints of finite-entropy systems [4–6]: information cannot be stored in an arbitrarily large number of independent degrees of freedom, and correlation functions cannot decay smoothly to zero forever [7].

This expectation is in direct tension with inflationary engineering. In slow-roll model building one can, within semiclassical effective field theory, tune the inflaton potential to realize an arbitrarily long quasi-dS stage with an arbitrarily large number of e-folds  $N$ . Each e-fold generates additional superhorizon modes that freeze out during inflation, implying an unbounded growth of cosmological information. This tension of dS is analogous to the black hole information problem.

In a post-reheating cosmology, this tension can be framed in terms of observables: a so-called CMB observer at post-reheating time  $t$  can access only the subset of modes that have re-entered the horizon by that time, while the formal long-time limit  $t \rightarrow \infty$  probes an ever larger set of inflationary modes. In parallel, one may regard  $N$  not as dynamical time inside the dS path integral but as a *state-preparation parameter* labeling a family of reheating-surface states  $|\Psi(N)\rangle$ . Varying  $N$  provides a theoretical diagnostic of how observables depend on the inclusion of increasingly many horizon-exited modes—precisely where the clash with finite entropy is expected to sharpen. In this work, instead of  $t$  and  $N$ , we will use  $k_{\min}$  and  $k_{\max}$  in the path-integral preparation of the state.

The gravitational path integral prepares a quantum state on the boundary of quasi-dS—reheating surface—by integrating over all possible past Euclidean geometries and field configurations given boundary conditions [8]. Although past time slices in path integral cannot be interpreted as real dynamics of inflation and observables inside dS are uncertain [4, 9], the state can be measured in a post-reheating flat region as discussed. The two observables based on different notions of time allow complementary scrutinizations of the state.

In a finite-entropy system, late-time correlators are not expected to decay indefinitely; rather, they should exhibit residual correlations [7] and, after appropriate averaging, ramp-and-plateau behavior [10–12]. A natural scale for the onset of such deviations is a dS analogue of the Page time: irreducible errors due to the finite number of states  $e^{-S_{\text{dS}}}$  ( $\propto e^{-1/G}$ , hence non-perturbative) can become order one when enhanced by an effective multiplicity of available states of order  $e^{S_{\text{dS}}}$  [13, 14]. However, horizon is also thought to be a chaotic fast-scrambling system, out of which information can leak far earlier than the Page time [15–17]. Determining the mechanism that supplies these non-perturbative corrections and how it manifests in correlators of cosmological interest are the central motivations of this work.

A concrete precedent comes from the black hole information problem [3, 18], where replica and bra-ket wormhole saddles modify semiclassical calculations and yield late-time behaviors consistent with unitarity [19, 20]. Inspired by this mechanism, we study whether analogous *bra-ket wormholes* [21, 22] contribute to correlators in dS-prepared states, in ways consistent with the finite-entropy constraints.

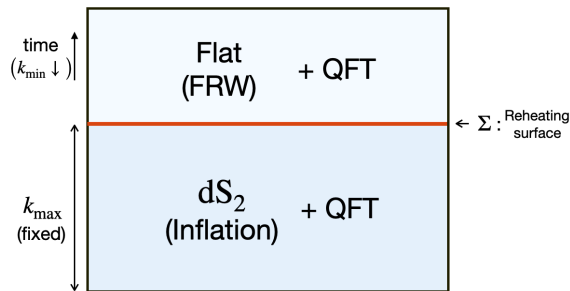


**Figure 1:** dS prepares a quantum state (of the scalar field) on its spatial boundary  $\Sigma$ , reheating surface, including effects from higher-topology wormholes. The state is then observable in the flat space afterwards without gravity. The observation utilizes two notions of time:  $k_{\max}$  and  $k_{\min}$ .

The paper is organized as follow. In Sec. 2, we introduce our calculation setup and the gravitationally prepared state with various consistency relations. In Sec. 3, we find bra-ket wormhole saddle at the next-to-leading order(NLO) in topological expansion. In Sec. 4, we calculate two-point correlators and discuss results of the two observables. Then we conclude with limitations and implications in Sec. 5.

## 2 Gravitationally prepared state at the end of inflation

As depicted in Fig. 1, we gravitationally prepare a state on the future spatial boundary  $\Sigma$  of dS space (Sec. 2.1), which is then observable in the flat space without gravity afterwards (Sec. 2.2). Thus, we assume finite dS, as a model of inflationary universe. On the contrary to black hole-AdS system, spacetimes with gravity turned on and off are timelike separated.

Gravitational path integral is said to gravitationally prepare a quantum state in the spatial boundary  $\Sigma$

$$\int^{\Sigma} Dg D\Phi e^{iS}, \quad (2.1)$$

where geometry  $g$  is fixed at  $\Sigma$  but quantum fields  $\Phi$  are left unspecified in general, so that the path integral is a functional of boundary field value  $\phi = \Phi|_{\Sigma}$ . The integral over  $g$  can often be approximated by a discrete sum over saddle geometries  $g_c$ .

The action is given by the scalar quantum field theory on 2-dimensional JT [23, 24] dS space

$$S = S_{\text{grav}} + S_{\text{QFT}}[g, \Phi], \quad (2.2)$$

$$S_{\text{grav}} = \frac{\varphi_0}{4G_2} \chi + \frac{1}{16\pi G_2} \left( \int \sqrt{-g} \varphi (R - 2) - 2 \int \sqrt{h} \varphi_b (K - 1) \right). \quad (2.3)$$

The dilaton  $\varphi$  fixes  $R = 2$  by its equation of motion, its reference value is larger than the boundary value  $\varphi_b \ll \varphi_0$ , which determines the 2d dS entropy  $S_{\text{dS}} = 2\varphi_0/4G_2$ .  $\chi$  is the

Euler characteristic (in the Lorentzian signature)

$$\chi = \frac{1}{4\pi} \left( \int \sqrt{-g} R - 2 \int \sqrt{h} K \right) = -i\chi_E, \quad \chi_E = 2 - 2g - n, \quad (2.4)$$

providing topological expansion of geometries  $e^{\frac{1}{2}S_{\text{ds}}\chi_E}$ . The QFT action for a real scalar matter field is given by a minimal one

$$S_{QFT}[g, \Phi] = \frac{1}{2} \int \sqrt{-g} (-g^{\mu\nu} \partial_\mu \Phi \partial_\nu \Phi - m^2 \Phi^2). \quad (2.5)$$

## 2.1 Gravitational state preparation, and consistency

To clarify notation and relative boundary conditions for bra and ket spaces, we rewrite gravitational state preparation while comparing with quantum mechanical bra-ket notation. Above all, we will consider only real fields on the boundary.

Define a gravitationally prepared ket state, in a given saddle geometry  $g_c$ , (up to normalization)

$$U|0\rangle = \int_0^\phi D\Phi e^{+i \int_0^t \mathcal{L}}, \quad (2.6)$$

where 0 refers to a boundary condition defining a state (essentially selected by the saddle geometry  $g_c$ , in the Euclidean regime), and the boundary condition for the bra slice (where measurements are made) is open except that it is at time  $t$ . On the left-hand side, we use corresponding quantum mechanical bra-ket notation, where  $U$  represents (both Euclidean and Lorentzian) path evolution of initial data  $|0\rangle$  to the ket slice at  $t$ . When this ket state is projected onto the field basis  $|\phi\rangle$  at  $t$ ,

$$\langle \phi | U | 0 \rangle = \int_0^\phi D\Phi e^{+i \int_0^t \mathcal{L}}. \quad (2.7)$$

This result might be interpreted as wavefunctional  $\Psi[\phi]$ . The gravitationally prepared bra state is then related by complex conjugation

$$\langle 0 | U^\dagger = \int_{0^*}^\phi D\Phi e^{-i \int_{0^*}^t \mathcal{L}} = \int^{0^*} D\Phi e^{+i \int_{t^*}^0 \mathcal{L}}, \quad (2.8)$$

using the elementary relation  $(\int_a^b dx f(x))^* = F^*(b^*) - F^*(a^*) = \int_{a^*}^{b^*} dx f^*(x)$ . The complex time variable is used to imply its analytic continuation. The latter form in Eq. (2.8) is useful when computing the elements of density matrix as one path integral

$$\rho \sim U|0\rangle\langle 0|U^\dagger \sim \int D\Phi e^{+i \int_{t^*}^t \mathcal{L}}, \quad \rho_{\phi\phi'} \sim \int_{\phi'^*}^\phi D\Phi e^{+i \int_{t^*}^t \mathcal{L}}. \quad (2.9)$$

One takeaway message is: *when bra and ket appear together, their boundary conditions are conjugated*. This is equivalent to having real eigenvalues of  $\rho$ , as you can check  $\rho_{\phi\phi'} = \rho_{\phi'\phi}^*$  using the above path-integral representation. Among multiple bras, conjugation is not needed.

In general, several saddle  $|0\rangle$  (or  $g_c$ ) contributions are summed in  $\rho$ . This is implicit in the notation of  $|0\rangle$ , which is actually a weighted superposition of various saddle contributions. In the path integral side, all possible past Euclidean saddles  $g_c$  (with given bra/ket boundary conditions) are summed up according to path integral philosophy.

Here comes an important distinction of gravitational path integral from quantum mechanics. For saddle geometries that do not connect bra and ket boundaries, the contribution to  $\rho$  is a product of bra and ket wavefunctions; this is same and clear in the quantum mechanical bra-ket notation. But path integral also allows wormhole geometries that connect bra and ket boundaries, which then cannot be factorized. This contribution may be subtle in terms of bra-ket notation of density matrix. And this wormhole contribution is what makes important deviation from mere quantum mechanical expectation based on unitarity and conservation of entropy, etc.

Expectation values of any observables  $\mathcal{O}$  are calculable using gravitational path integral

$$\text{Tr}[\mathcal{O}\rho] = \langle 0|U^\dagger\mathcal{O}U|0\rangle \sim \int D\phi \int_{\phi^*}^{\phi} D\Phi \mathcal{O} e^{+i\int_{t^*}^t \mathcal{L}}, \quad (2.10)$$

where  $D\phi = \Pi_k d\phi_k$  on the boundary fields. Various wormhole contributions are implicit as discussed. The two-point correlation of scalar matter field, which is our main interest, can be calculated by  $\mathcal{O} = \phi(x)\phi(y)$  at the 1D spatial boundary at  $t$ .

**Euclidean regime.** The time contour can be analytically continued to the complex plane, given the fixed boundary real time. Mathematically, it is a trick to do integral by finding out (complex) saddle geometries.

Physically, Euclidean regime is necessary to prepare states on the boundary. Without any imaginary parts in the time contour, the path integral is mere unitary evolution. Technically, the real part of action  $S$  in  $e^{iS}$  on the bra boundary is cancelled by that on the ket boundary; unitary evolution. Only the imaginary part of  $S$  can lead to non-trivial states.

Not only time, but fields can also be complexified, just as another trick to do integral and solve EoMs. Complex fields can also provide extra contributions to states. But time's analytic continuation and fields' complexifications are not arbitrary, subject to several consistency conditions.

**Probability interpretation.** To interpret path integral as a partition function, one shall have a conserved probability. The gravitationally prepared state, being a solution of Wheeler-DeWitt (WDW) equation, has a conserved norm if the classicality condition is satisfied [25, 26]

$$|\nabla_A \text{Im}(S_c)| \ll |\nabla_A \text{Re}(S_c)| \quad (2.11)$$

for the action  $S_c = S[g_c, \Phi_c]$  evaluated on a saddle  $\{g_c, \Phi_c, \dots\}$ .  $A$  represents the min-superspace  $\{g, \Phi, \dots\}$ . Then, the probability  $P \approx |\Psi|^2 = e^{-2\text{Im}(S_c)}$  is conserved (and

positive definite) along the trajectory  $\nabla_A \text{Re}(S_c)$ . The classicality condition Eq. (2.11) is reportedly equivalent to the reality condition on the boundary field values [26, 27],

$$\text{Im}(g_c) \ll \text{Re}(g_c), \quad \text{Im}(\Phi_c) \ll \text{Re}(\Phi_c), \quad \dots \quad (2.12)$$

In all these, actions and fields are boundary quantities, expressed by boundary values in path integral. This is so because it is only the boundary state (the result of path integral) which becomes a member of WDW solutions, living on the minisuperspace.

Note that this approach of defining a state does not generally have a global consensus of time. This becomes particularly subtle in dS, as it does not have asymptotic flat regions.

**Relaxed Kontsevich-Segal-Witten condition.** For path integral to be convergent, the KSW condition requires the coefficient of field-quadratic term to be negative [28, 29]. Originally, this condition was required to be true on each point on the time contour. This is expressed as a condition on the metric components:  $\sum_i |\arg(g_{ii})| < \pi$ . For example, Lorentzian Minkowski space saturates this limit as  $g_{tt} = -1 + \epsilon$  with the Feynman prescription  $\epsilon > 0$  [29]. As we will see, our wormhole solution does not obey this strict KSW condition.

However, we suggest a relaxed condition, which requires only the result of path integral

$$\int^\phi D\Phi e^{iS[g_c, \Phi]} \propto e^{-I\phi^2}, \quad \text{Re}(I) > 0 \quad (2.13)$$

to be convergent, instead of requiring a minus sign point-wisely. Thus,  $\text{Re}(I)$ , obtained from the integral of the on-shell Lagrangian along the time contour, should be positive. We confirm this numerically for our wormhole solutions.

**Hartle-Hawking geometry prepares the Bunch-Davies vacuum state.** The idea that a Euclidean geometry with right boundary condition determines the quantum state on the boundary (let alone the possibility of wormholes) was first and wonderfully realized by the no-boundary proposal by Hartle and Hawking [8]. This suggests that the leading contribution would be from a Euclidean hemisphere smoothly connected to the upper half of (the global coordinate of) the Lorentzian dS. This geometry is topologically leading order and is the most natural analytic continuation of the global coordinate. Most remarkably, the regularity of fields on the South pole successfully reproduces the unique Bunch-Davies vacuum on the Lorentzian part. See Sec. 3.1 for more detailed introduction.

## 2.2 Observation of dS prepared state, notion of time

**Post-inflationary observation.** Our situation in Fig. 1 is interpreted as inflation prepares a quantum state of the universe and scalar field (representing inflaton or the energy density fluctuation) on the reheating surface  $\Sigma$ , which is subsequently evolved into the post-inflationary FRW space. This state is observable by post-inflationary observers, e.g. by CMB and large scale structures.

As emphasized in [14, 30–32], this setup provides an operational or observational meaning to entropy, correlations, and other quantum properties of dS prepared state.

From the so called CMB observer’s point of view, observed properties of dS state change with time, as successively smaller Fourier modes of quantum fields (larger wavelength) re-enter horizon. The measured entropy also grows, and eventually becomes conflict with the finite dS entropy. Presumably, wormhole effects would cure this conflict, just like in the black hole case. In Sec. 4.3, we will show that wormhole effects encoded in various Fourier modes of dS state indeed make CMB observation consistent with unitarity and complementarity.

**Another notion of “time”.** We are dealing with approximate dS, in which full isometries are slightly broken due to the end of inflation. This breaking naturally brings in the notion of “time” (during inflation), both as a cutoff theoretically and as duration phenomenologically. We emphasize that we do not study the dynamics of quantum states inside dS (during inflation). But the quantum state prepared at the end of inflation does depend on the cutoff or the total amount of inflation. By comparing quantum states of different universes with different duration, we might also be able to discuss some kind of time dependence of gravitationally prepared states. This also allows to discuss phase transition into wormhole dominance phase. As will be discussed in Sec. 4.4, this way of ‘observing’ dS state is also consistent with resolving dS information problem.

### 3 Wormholes for two-point correlations of scalar QFT

#### 3.1 Equations of motion and boundary conditions in the global coordinate

We use the global coordinate in this work ( $N = 1$  minisuperspace with constant-time horizontal surfaces as foliation)

$$ds^2 = -dt^2 + a(t)^2 d\theta^2, \quad \theta \in [0, 2\pi). \quad (3.1)$$

To calculate QFT states on the future surface under dynamic gravity, we use gravitational path integral to evolve initial data (essentially selected by saddle geometry) on a Cauchy surface in the past Euclidean regime into future data on the physical boundary. To this end, the global coordinate is most flexible in analytically continuing the geometry from Lorentzian to Euclidean region. Both matter fields and the metric remain regular in this coordinate. The initial surface of Lorentzian dS is smoothly and naturally glued to the Euclidean region, just like the leading-order Hartle-Hawking(HH) no-boundary geometry.

In comparison, for CFT states (as often studied in literature), geometry plus CFT alone can determine the quantum state, while the path integral provides topological expansion of saddle geometries. Earlier works with CFT chose various coordinates (e.g. global in [32] and Milne in [21, 22]), as CFTs do not need to be solved analytically with full initial conditions. However, our goal is to obtain correlation functions of QFT matter fields, and for this we must solve EoMs in a foliation that covers both the entire initial surface and the late-time surface, at ease.

**EoMs.** The variations of the gravity part of action Eq. (2.2) with respect to the dilaton  $\varphi$  and metric field  $g_{\mu\nu}$  yield the following EoMs,

$$R = 2, \quad (\nabla_\mu \nabla_\nu + g_{\mu\nu})\varphi = -8\pi G_2 T_{\mu\nu}^M, \quad (3.2)$$

with boundary conditions at the time  $t_\epsilon = \log(2/\epsilon)$  corresponding to the bra or ket space,

$$ds_b^2 = \frac{d\theta^2}{\epsilon^2}, \quad \varphi_b = \frac{\varphi_r}{\epsilon}. \quad (3.3)$$

The size of boundary is  $\ell = 2\pi a(t_\epsilon) = 2\pi/\epsilon$ . The metric EoM reduces to

$$\ddot{a}(t) = a(t), \quad (3.4)$$

which admits solutions expressed in terms of hyperbolic functions.

In the given geometry  $a(t)$ , the bulk scalar field,  $\Phi(t, \theta) = \sum_k e^{ik\theta} \Phi_k(t)$ , obeys the following EoM from the matter action Eq. (2.5)

$$\ddot{\Phi}_k(t) + \frac{\dot{a}(t)}{a(t)} \dot{\Phi}_k(t) + \left( \frac{k^2}{a(t)^2} + m^2 \right) \Phi_k(t) = 0. \quad (3.5)$$

At late time near boundary, the asymptotic form of solutions for  $\Phi_k(t)$  can be generally expressed as

$$\Phi_k(t) \simeq \frac{\phi(k)}{u(t_\epsilon)} (\phi(k) a(t)^{-\Delta_-} + \mathcal{O}(k) a(t)^{-\Delta_+}), \quad \Delta_\pm \equiv \frac{1}{2} \pm \sqrt{\frac{1}{4} - m^2}, \quad (3.6)$$

where  $u(t_\epsilon) = \phi(k) \epsilon^{\Delta_-} + \mathcal{O}(k) \epsilon^{\Delta_+}$  from the boundary condition  $\Phi_k(t_\epsilon) = \phi(k)$ .  $\mathcal{O}(k)$  is the piece that depends on saddle geometry  $g_c$  and boundary conditions; thus, when saddle specific results are necessary, we will denote it by  $\mathcal{O}^c(k)$  with the superscript  $c$ . But it is always  $\mathcal{O}(k) \propto \phi(k)$ . The on-shell action becomes a boundary term

$$S_{\text{QFT}} = \pi \sum_k a(t) \Phi_{-k}(t) \partial_t \Phi_k(t) \Big|_{t_\epsilon} = -2\nu\pi a(t_\epsilon)^{\Delta_-} \sum_k \phi(-k) \mathcal{O}(k). \quad (3.7)$$

Since  $\mathcal{O}(k) \propto \phi(k)$ , the action is quadratic in fields  $S_{\text{QFT}} \sim \sum_k \mathcal{A}_k \phi(k) \phi(-k)$ . When bra and ket appear together in density matrix or two-point functions, only the imaginary part  $\text{Im}(\mathcal{A}_k)$  survives in  $i(S - S^*)$  (by the relative conjugacy of bra and ket boundary conditions) and determines two-point correlations. This structure of solution is common to all dS geometries.

The general structure that  $\mathcal{O}(k)$  carries all saddle-dependent information and correlation information is in parallel with the AdS/CFT or dS/CFT correspondence. There,  $\mathcal{O}(k)$  becomes a boundary CFT operator. By QFT calculation in a non-trivial wormhole geometry, we explicitly check that this structure is still valid.

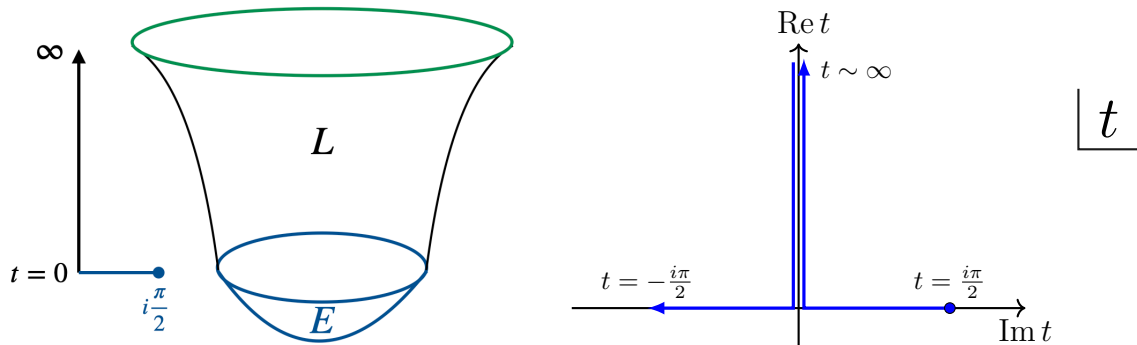


**Figure 2:** (Left:) HH no-boundary saddle in Eq. (3.8). (Right:) Its contribution to the density matrix in Fig. 4 by a single path integral.

**Leading-order no-boundary saddle.** As alluded, HH no-boundary geometry is a unique and natural saddle at LO. The geometry is given by

$$\begin{aligned} ds_{\text{Eucl.}}^2 &= d\tau^2 + \alpha^2 \cos^2(\tau) d\theta^2, \quad \tau \in [0, \pi/2], \\ ds_{\text{Loren.}}^2 &= -dt^2 + \alpha^2 \cosh^2(t) d\theta^2, \quad t \in [0, \infty), \end{aligned} \quad (3.8)$$

as depicted in Fig. 2 left panel. The Euclidean hemisphere ( $\chi_E = 1$ ) is smoothly transitioned to the global coordinate at  $t = 0$ . The South pole is located at  $t = i\tau = i\pi/2$ , at which fields are required to be regular. This natural boundary condition reproduces the Bunch-Davies vacuum on the future Lorentzian boundary. Exact solutions and on-shell actions are collected in Appendix A.1. Its contribution to the density matrix can be calculated by a single path integral along the time contour shown in Fig. 2 right panel.

### 3.2 Naive bra-ket wormholes do not exist at NLO

**Two-boundary connected geometry.** To find a bra-ket wormhole (in Sec. 3.3), we start with a two-boundary connected geometry. Depending on the nature of the two boundaries, this geometry can be called a bra-ket, bra-bra, or ket-ket wormhole. The topology at NLO is cylinder ( $\chi_E = 0$ ).

The only viable two-boundary solution for the scale factor is a complexified one given by

$$a(t) = \frac{1}{2} (e^t + e^{i\tau_0 - t}). \quad (3.9)$$

The complex time contour connecting the two boundaries is depicted in Fig. 3. The geometry asymptotes to the real global coordinate  $a(t) \rightarrow \cosh t$  toward each boundary  $t \rightarrow \infty$  and  $t \rightarrow -\infty + i\tau_0$ . At  $t = 0$ , a Euclidean cylinder is glued via analytic continuation  $t = i\tau$  with  $\tau \in [0, \tau_0]$ , whose timelike length  $\tau_0$  characterizes the Euclidean wormhole.

Unlike usual analytic continuation of time variable alone, we complexify the functional form of  $a(t)$  too (Eq. (3.9)). The complexification is needed to have a solution. If two

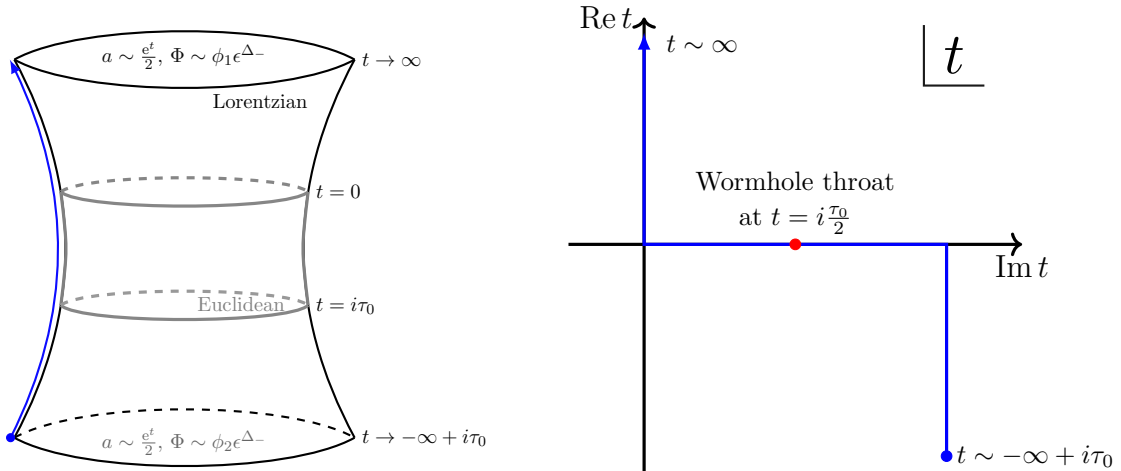


**Figure 3:** 2-boundary wormhole saddle at NLO in Eq. (3.9), which is a building block of the bra-ket wormhole in Fig. 4 and Sec. 3.3. This by itself can only be a ket-ket or bra-bra wormhole because continuity of fields in the throat disallows proper boundary conditions for bra-ket wormholes (Sec. 3.2).

boundaries are simply connected through the periodic complex time contour  $t = 0 \sim 2\pi i$ , the geometry in the global coordinate becomes factorized into two HH hemispheres rather than a single connected bra-ket wormhole. This is different from the Milne coordinate and AdS, in which a doughnut-shaped wormhole along the periodic direction is obtained.

The complexified  $a(t)$  may raise concerns. It is still imaginary along the real time line, and is not exactly real on the future cutoff surface at  $t_\epsilon$ . However, it still satisfies the classicality condition in Eq. (2.12)

$$a(t) \sim \dot{a}(t) \sim \frac{1}{2}e^t \quad (3.10)$$

at late times  $t \gg 1$ , in that  $a(t)$  and its conjugate momentum are almost real on the boundary. This was enough for probability interpretation.

The complex-valued scale factor induces additional complex phase, which only worsens the KSW condition and violates the condition at every point along the time contour. Nevertheless, the kernel resulting from the path integral remains positive so that the relaxed KSW is satisfied. We have checked this numerically.

The vacuum dilaton solution on this saddle geometry is

$$\varphi(t) = \varphi_r e^{i\tau_0/2} \sinh\left(t - \frac{i\tau_0}{2}\right). \quad (3.11)$$

Here, we neglect the contribution from the matter stress-energy tensor since it is exponentially suppressed at late times and subleading in  $G_2$ .

The boundary extrinsic curvature on the ket side is given by

$$K_{\text{ket}} = 1 - \epsilon^2 \left( \{f_{\text{ket}}(\theta), \theta\} + e^{i\tau_0} \frac{f'_{\text{ket}}(\theta)^2}{2} \right), \quad (3.12)$$

with the bra side similarly by complex conjugation. The corresponding on-shell action is

$$\begin{aligned} iS_{\text{grav}} &= \frac{i\varphi_r}{8\pi G} \int_0^{2\pi} d\theta \left[ \left( \{f_{\text{ket}}(\theta), \theta\} + e^{i\tau_0} \frac{f'_{\text{ket}}(\theta)^2}{2} \right) - \left( \{f_{\text{bra}}(\theta), \theta\} + e^{-i\tau_0} \frac{f'_{\text{bra}}(\theta)^2}{2} \right) \right] \\ &= -\frac{\varphi_r}{4G} \sin \tau_0, \end{aligned} \quad (3.13)$$

where in the final line  $f_{\text{ket}}(\theta) = f_{\text{bra}}(\theta) = \theta$  was used.<sup>1</sup>

Note that the gravity part  $S_{\text{grav}}$  is not exactly real on the boundary so that the gravity contribution is not cancelled between bra and ket sides in Eq. (3.13). This is due to the complexified  $a(t)$ . This is anyway consistent as discussed, and is also numerically small since  $\varphi_r \ll \varphi_0$ .

**Matter solution.** For QFT scalar matter fields, we impose Dirichlet boundary conditions on both boundaries at  $t = t_\epsilon, -t_\epsilon + i\tau_0$ ,

$$\Phi(t_\epsilon, k) = \phi_1(k), \quad \Phi(-t_\epsilon + i\tau_0, k) = \phi_2(k). \quad (3.14)$$

A solution to the scalar field EoM can be expressed similarly to the HH solution,

$$\Phi(t, k) = \phi_1(k) \frac{v_k(t)}{v_k(t_\epsilon)} = \phi_2(k) \frac{v_k(t)}{v_k(-t_\epsilon + i\tau_0)}. \quad (3.15)$$

$v_k(t)$  is given in Appendix A. By employing the asymptotic form of solutions in Eq. (3.6)

$$v_k(t) \simeq \phi(k) a(t)^{-\Delta_-} + \mathcal{O}^{WH}(k) a(t)^{-\Delta_+}, \quad (3.16)$$

the matter action is evaluated as (Eq. (3.7))

$$\begin{aligned} iS_{\text{QFT}}[g_c, \Phi_c] &= i\pi \sum_k a_c(t) \partial_t \Phi_c(t, k) \Phi_c(t, -k) \Big|_{-t_\epsilon + i\tau_0}^{t_\epsilon} \\ &= -2i\pi\nu \sum_k \left( \frac{2\pi}{\ell} \right)^{-\Delta_-} \left[ \phi_1(-k) \mathcal{O}_1^{WH}(k) + \phi_2(-k) \mathcal{O}_2^{WH}(k) \right]. \end{aligned} \quad (3.17)$$

On each boundary, say 1,  $\mathcal{O}_1^{WH} = \tilde{a}\phi_1 + \tilde{b}\phi_2$ , where  $\tilde{b}$  parametrizes the mixing between two boundary field values  $\phi_1$  and  $\phi_2$ . Consequently, the resulting action is quadratic in the boundary values  $\phi_{1,2}$ . This mixing is critical in understanding various properties of wormholes, as will be discussed throughout.

Although complex in bulk,  $\Phi$  also obeys the classicality condition. From the asymptotic form in Eq. (3.16), the only piece that might contain sizable imaginary part on the boundary (hence, problematic) is  $\mathcal{O}^{WH}(k)$ . But this second term is exponentially smaller than the first term. Likewise, its conjugate momentum brings only  $\Delta_\pm$  factors to the front, which is not of exponential in size. Thus,  $\Phi$  and its conjugate momentum are almost real on the boundary.

---

<sup>1</sup>Quantum corrections from fluctuations of the Schwarzian mode  $f(\theta) = \theta_0 + \delta\theta$  are known exactly [33, 34], but are not included here.

$$\rho(\phi_1, \phi'_1) = \text{[Diagram 1]} + \int \mathcal{D}\phi_2 \text{[Diagram 2]}$$

**Figure 4:** Gravitational path integral calculation of density matrix, in the field basis. The leading contribution is a product of HH states, while the NLO contribution is the effective bra-ket wormhole, which is obtained by joining two 2-boundary wormholes in Fig. 3 and tracing out unobservable separate universe (denoted with  $\phi_2$ ); see Sec. 3.3.

**This is not a bra-ket wormhole.** As discussed in Sec. 2.1, for the two boundaries to be identified as a bra and a ket (thus forming a bra-ket wormhole), bulk fields on either side of wormhole throat was required to be complex conjugate of each other. But our two-boundary wormhole above does not satisfy this boundary condition. This can be checked directly or as following.

The shift  $t \rightarrow -t + i\tau_0$  maps the bulk on one side to the other side in the wormhole geometry. The explicit solution that we found is symmetric under this without complex conjugation

$$a(t) = a(-t + i\tau_0). \quad (3.18)$$

The matter field saddle inherits the same symmetry, since its EoM is determined by this background. Therefore, this two-boundary geometry cannot be a bra-ket wormhole. But this geometry can still be a bra-bra or a ket-ket wormhole. In the next subsection, we combine these bra-bra and ket-ket wormholes to construct a bra-ket wormhole.

### 3.3 Bra-ket wormhole by tracing out unobservable universe

We construct an effective bra-ket wormhole by combining a bra-bra and a ket-ket wormhole, as depicted in Fig. 4. The upper half, which is a ket-ket wormhole, is a complex conjugate of the lower half, which is a bra-bra wormhole, so that the bra-ket relative conjugacy condition is effectively satisfied. Each bra-bra or ket-ket wormhole is thought to produce two separate universes, with independent boundary conditions  $\phi_1$  and  $\phi_2$ . Then the unobservable universes (say with  $\phi_2$ ) from bra-bra and ket-ket wormholes are joined and traced over. This results in a proper bra-ket wormhole, that contributes to the desired density matrix

$$\rho[\phi_1, \phi'_1] = \int \mathcal{D}\phi_2 \rho[\{\phi_1, \phi_2\}, \emptyset] \rho[\emptyset, \{\phi'_1, \phi_2\}]. \quad (3.19)$$

This idea was also suggested by [35] in a situation where direct bra-ket wormholes did not exist.

Let us compute more concretely. The path integral over each bra-bra and ket-ket wormhole results in each density matrix

$$\int_{\Phi_{\partial}=(\phi_1,\phi_2)} \mathcal{D}\Phi \mathcal{D}g e^{iS[g,\Phi]} \simeq e^{iS_c[g_c,\Phi_c]}, \quad (3.20)$$

where the on-shell action evaluated on the saddle  $(g_c, \Phi_c)$  is in the form of

$$\begin{aligned} iS_c[g_c, \Phi_c] &= i\pi \sum_k a_c(t) \partial_t \Phi_c(t, k) \Phi_c(t, -k) \Big|_{-t_c+i\tau_0}^{t_c} \\ &= - \sum_k \left\{ a_k \phi_1(k) \phi_1(-k) - [b_k \phi_1(k) \phi_2(-k) + c.c.] + a_k \phi_2(k) \phi_2(-k) \right\}. \end{aligned} \quad (3.21)$$

Here,  $a_k, b_k$  are the constants determined by bulk scalar solution  $\Phi_c$ ; see Appendix A.2 for exact expressions. By combining bra-bra and ket-ket states, i.e.  $iS_c[\Phi_c] - iS_c^*[\Phi_c^*]$ , the total density matrix is in the form of (for each  $k$ -mode)

$$\int \mathcal{D}\phi_2 \exp \left[ -\alpha_k |\phi_1|^2 + \beta_k (\phi_1^* \phi_2 + \phi_1 \phi_2^*) - \alpha_k |\phi_2|^2 \right] \propto \exp \left[ - \left( \alpha_k - \frac{\beta_k^2}{\alpha_k} \right) |\phi_1|^2 \right], \quad (3.22)$$

where  $\alpha_k = 2\text{Re}(a_k)$  and  $\beta_k = 2\text{Re}(b_k)$ . This is for each  $k$ -mode. As discussed, the action is quadratic in field, and its coefficient leads to the two-point correlation at leading order.

**Consistencies.** This geometry obeys the classicality condition, simply because each bra-bra and ket-ket does so. The strict KSW is still not obeyed, but we checked numerically that the relaxed KSW is satisfied. This means that the coefficient of quadratic term for each  $k$  is positive:  $\alpha_k > \beta_k$  for all  $k$ , from Eq. (3.22).

Moreover, for large  $k > k^*$ , the wormhole action in Eq. (3.22) agrees with that of HH. This must be so because modes that are shorter than the wormhole scale ( $\tau_0$ ) or the curvature of space are insensitive to the global geometry. This means that  $\beta_k \rightarrow 0$  for large  $k > k^*$ .

As a result of these consistencies, the effective coefficient of quadratic term is reduced for small  $k$ :  $\alpha_k \rightarrow \alpha_k - \beta_k^2/\alpha_k$  from Eq. (3.22). This enhances low- $k$  (long-range) correlations. As will be discussed in Sec. 4.2, this enhancement will be critical in phase transition to wormhole dominance.

**Never ending (bra-bra)+(ket-ket) chains?** One may wonder if our mechanism of forming an effective bra-ket wormhole by joining bra-bra and ket-ket wormholes can be extended by joining even more chains of bra-bra and ket-ket wormholes. They are indeed legible contributions. But, as detailed in Appendix D, adding  $n$  such chains increases the action in proportion to  $\propto n$  so that they are exponentially suppressed. Creating longer and more complex wormholes essentially costs more resources. We ignore these contributions.

### 3.4 Stabilization of wormholes

The partition function from each  $k$  mode

$$\int D\phi_k e^{-a_k \phi_k^2} = \sqrt{\frac{1}{a_k}} = e^{-\frac{1}{2} \log a_k}, \quad (3.23)$$

is diverging as  $\tau_0 \rightarrow 0$  since  $a_k \simeq c_k \tau_0$  for small  $\tau_0$ . In this  $\tau_0 \rightarrow 0$  limit (equivalently, in the limit of infinite temperature), the partition function corresponds to merely counting total number of states, as Boltzmann suppression of high-energy states is absent. In the finite-entropy system, this must be finite and, moreover, bounded by about  $e^{S_{\text{dS}}}$ . So the divergence sounds like a pathology of semiclassical effective theory. Further, this problem is related to the stabilization of the wormhole;  $\tau_0 = 0$  means that the size of Euclidean geometry vanishes. If wormholes are to make sizable contributions,  $\tau_0$  shall be stabilized to some non-zero finite value. The wormhole stabilization is a more general problem in dS, even with CFT matter in the bulk [21, 22, 36].

In the random state model of quantum gravity [37], wormholes indeed turn out to be stabilized; without encountering any divergences, this model successfully reproduces the expected properties of correlation functions in the wormhole dominant phases. Also, in Ref. [22], Wigner distribution of observables also provided some stabilizing force. Accepting these general expectations, we will simply assume a non-zero finite value of  $\tau_0 = 0.01$  in our numerical calculations. But true saddle points shall be in relation to  $S_{\text{dS}}$  as will be discussed, which we leave for future works.

Naively, the divergence at  $\tau_0 \rightarrow 0$  seems to be regularized by  $\zeta$  function

$$\int D\phi e^{-\sum_k a_k \phi_k^2} = \prod_k \sqrt{\frac{\pi}{a_k}} \tag{3.24}$$

$$\rightarrow \exp \left[ \frac{1}{2} \left( 2 \sum_{k \in \mathbb{N}} 1 + 1 \right) \log \tau_0 + \dots \right] = \exp \left( \frac{1}{2} (2\zeta(0) + 1) \log \tau_0 + \dots \right)$$

where the ellipsis indicates  $\tau_0$ -independent finite constants. This is valid for small  $\tau_0$  (where  $a_k \propto \tau_0$  linearly). One can regulate the sum over natural numbers using the  $\zeta$  function with  $\zeta(0) = -\frac{1}{2}$ , and this exactly cancels the  $\log \tau_0$  divergence. However, this infinite sum is not consistent with the cutoff  $k_{\text{max}}$  of semiclassical effective theory, which will be introduced and utilized in our observables. Thus, we do not take this possibility seriously.

**Fermions added.** We remark that both problems can be explicitly resolved by introducing a Majorana fermion  $\psi$  (two real components) for each complex scalar field  $\phi$ . The Gaussian integral over anticommuting fields leads to the opposite  $\tau_0$  dependence

$$\int D\psi_k D\bar{\psi}_k e^{-b_k \bar{\psi}_k \psi_k} = b_k = e^{+\log b_k}, \tag{3.25}$$

where  $b_k \sim \tau_0$  as  $\tau_0 \rightarrow 0$ . The detailed calculation is described in Appendix B. Thus, for each mode  $k$ , the scalar ( $\sim e^{-\tau_0}$ ) and fermion ( $\sim e^{+\tau_0}$ ) contributions cancel the leading  $\log \tau_0$  divergence. In a sense, fermions repel wormholes to shrink completely. The residual dependence on  $\tau_0$  also leads to non-zero finite saddle value of  $\tau_0$ , essentially due to the same opposite dependence. An example result in Fig. 13 shows that the saddle is located at  $\tau_0 \simeq 10^{-3}$ .

However, this mechanism of stabilization cannot be complete as it does not depend on the gravity action. This will be discussed later in Fig. 12. Thus, we do not take this

resolution with extra fermions seriously. Rather, in this study, we simply take the fixed value  $\tau_0 = 10^{-2}$ .

## 4 Observables of bra-ket wormholes

### 4.1 Notions of time: $k_{\max}$ and $k_{\min}$

In post-inflationary observation of dS prepared state, only those modes of scalar field that became superhorizon by the end of inflation will be classicalized and observable. We introduce upper limit on the observable Fourier modes of scalar field,  $k_{\max}$ , as the largest  $k$ -mode that existed horizon ( $1/H$ ) by the end of inflation

$$\frac{2\pi a(t_\epsilon)}{H k_{\max}} = \frac{1}{H} \quad \rightarrow \quad k_{\max} = 2\pi a(t_\epsilon). \quad (4.1)$$

$k_{\max}$  appears in path integral calculation of correlation functions in the following way

$$\begin{aligned} \langle \phi_k \phi_{-k} \rangle &= \frac{\int^{k_{\max}} \mathcal{D}\phi \phi_k \phi_{-k} \left\{ e^{S_{\text{dS}}} \exp\left(-4\pi \sum_q^{k_{\max}} \text{Im} \mathcal{A}_q^{\text{HH}} \phi_q \phi_{-q}\right) + \exp\left(-4\pi \sum_q^{k_{\max}} \text{Im} \mathcal{A}_q^{\text{WH}} \phi_q \phi_{-q}\right) \Big|_{\tau_0} \right\}}{\int^{k_{\max}} \mathcal{D}\phi \left\{ e^{S_{\text{dS}}} \exp\left(-4\pi \sum_q^{k_{\max}} \text{Im} \mathcal{A}_q^{\text{HH}} \phi_q \phi_{-q}\right) + \exp\left(-4\pi \sum_q^{k_{\max}} \text{Im} \mathcal{A}_q^{\text{WH}} \phi_q \phi_{-q}\right) \Big|_{\tau_0} \right\}} \\ &= \frac{\frac{1}{8\pi \text{Im} \mathcal{A}_k^{\text{HH}}} \prod_q^{k_{\max}} \sqrt{\frac{\pi}{4\pi \text{Im} \mathcal{A}_q^{\text{HH}}}} + e^{-S_{\text{dS}}} \frac{1}{8\pi \text{Im} \mathcal{A}_k^{\text{WH}}(\tau_0)} \prod_q^{k_{\max}} \sqrt{\frac{\pi}{4\pi \text{Im} \mathcal{A}_q^{\text{WH}}(\tau_0)}}}{\prod_q^{k_{\max}} \sqrt{\frac{\pi}{4\pi \text{Im} \mathcal{A}_q^{\text{HH}}}} + e^{-S_{\text{dS}}} \prod_q^{k_{\max}} \sqrt{\frac{\pi}{4\pi \text{Im} \mathcal{A}_q^{\text{WH}}(\tau_0)}}}. \end{aligned} \quad (4.2)$$

Here,  $\mathcal{D}\phi = \prod_k d\phi_k$  on boundary modes. We sum only observable superhorizon modes  $k \leq k_{\max}$  both in the path-integral measure and in the action sum. Subhorizon modes are quantum corrections, affecting correlations of superhorizon modes only through loop effects. These are not expected to be significant after inflation ends.

Based on Eq. (4.2), Observable 1 considers two-point correlations in the dS prepared state with fixed  $k_{\max}$ :  $\langle \phi_k \phi_{-k} \rangle$  for  $0 \leq k \leq k_{\max}$  and its spatial correlation

$$\langle \phi(\theta) \phi(0) \rangle = \sum_{k \in \mathbb{Z}}^{k_{\max}} e^{ik\theta} \langle \phi_k \phi_{-k} \rangle. \quad (4.3)$$

By  $k_{\max}$ , we do not mean to study dynamics during inflation (inside dS);  $k_{\max}$  is a fixed quantity for each dS universe. However, the quantum state at the end of inflation does depend on  $k_{\max}$ . Thus, varying  $k_{\max}$  means comparing states from different universes with different duration of inflation. In this way, we can discuss some kind of time dependence, such as when the phase transition to wormhole dominance occurs.

$k_{\max}$  happens to be the same as the cutoff of dS space:  $k_{\max} = 2\pi/\epsilon = 2\pi a(t_\epsilon)$  from Eq. (3.3). The introduction of  $\epsilon$  did not force to introduce  $k_{\max}$ . It is inflationary physics that requires to introduce  $k_{\max}$  and provides absolute physical meaning.

Observable 2, on the other hand, considers CMB-like two-point correlations, hence only among those modes that have successively re-entered horizon by given time. This

introduces another notion of time:  $k_{\min}$  as the smallest Fourier modes of scalar fields that have re-entered by given time

$$\langle \phi(\theta)\phi(0) \rangle = \sum_{k=k_{\min}}^{k_{\max}} e^{ik\theta} \langle \phi_k \phi_{-k} \rangle, \quad (4.4)$$

with  $\langle \phi_k \phi_{-k} \rangle$  given by Eq. (4.2). The farther future from reheating, the smaller  $k_{\min}$  and the more modes have re-entered horizon. By varying  $k_{\min}$ , we really mean to study the time-dependence of CMB observation of the given prepared state by a single observer.

$k_{\min}$  appears only in the Fourier sum in Eq. (4.4), but not in the path integral measure and the action sum in Eq. (4.2). The state—particular set of Fourier modes with weights—is already fixed by  $k_{\max}$ -path integral. It is only a matter of which modes among them to combine for correlation observables.

In summary, the two notions of time provide complementary diagnoses of the dS prepared state; one as a proxy of the time-dependence of dS gravitational non-perturbative effects, and the other as a CMB observation clock. Each observable shall make sense by itself, as some kind of dS complementarity.

## 4.2 Phase transition to wormhole dominance

If wormholes are to resolve information problem, they shall presumably begin to dominate at some late stage of dS. How does this phase transition between different dominant saddles occur in our solution? We discuss its basic mechanism, which will be realized slightly differently in our two observables.

See Eq. (4.2) second line numerator. Which saddle dominates is essentially a question of which of the following term is larger

$$\prod_q^{k_{\max}} \sqrt{\frac{1}{\text{Im}\mathcal{A}_q^{HH}}} \quad \text{vs.} \quad e^{-S_{\text{dS}}} \cdot \prod_q^{k_{\max}} \sqrt{\frac{1}{\text{Im}\mathcal{A}_q^{WH}}}. \quad (4.5)$$

For the latter wormhole effect to dominate, it is critical to have  $1/\text{Im}\mathcal{A}_k^{HH} < 1/\text{Im}\mathcal{A}_k^{WH}$ . Then, by having many enough modes (with some large enough  $k_{\max}$ ), the multiplication of  $1/\text{Im}\mathcal{A}_q^{WH}$  terms can overcome topological suppression  $e^{-S_{\text{dS}}}$ . If true, in other words, only long enough inflation would ever experience the phase of wormhole dominance. This kind of competition between the number of modes versus topological suppression, at least qualitatively agrees with the general mechanism of resolving information problem via connected geometries [19, 20].

As a result, depending on the ratio  $Z_{\text{rat}} \equiv \prod_q^{k_{\text{max}}} \sqrt{\frac{\text{Im}\mathcal{A}_q^{\text{HH}}}{\text{Im}\mathcal{A}_q^{\text{WH}}}}$  vs.  $e^{-S_{\text{dS}}}$ ,

$$\begin{aligned} \langle \phi_k \phi_{-k} \rangle &= \frac{1}{1 + e^{-S_{\text{dS}} Z_{\text{rat}}}} \frac{1}{8\pi \text{Im} \mathcal{A}_k^{\text{HH}}} + \frac{e^{-S_{\text{dS}} Z_{\text{rat}}}}{1 + e^{-S_{\text{dS}} Z_{\text{rat}}}} \frac{1}{8\pi \text{Im} \mathcal{A}_k^{\text{WH}}} \\ &\simeq \begin{cases} \frac{1}{8\pi \text{Im} \mathcal{A}_k^{\text{HH}}}, & Z_{\text{rat}} \ll e^{S_{\text{dS}}}, \\ \frac{1}{8\pi \text{Im} \mathcal{A}_k^{\text{WH}}}, & Z_{\text{rat}} \gg e^{S_{\text{dS}}}. \end{cases} \end{aligned} \quad (4.6)$$

We denote the critical point by  $k_{\text{max}} = k_{\text{max}}^c$ , where  $Z_{\text{rat}} = e^{-S_{\text{dS}}}$ . This is where phase transition occurs.

In our bra-ket wormhole solution, as discussed in Sec. 3.3,  $\mathcal{A}_k^{\text{WH}} < \mathcal{A}_k^{\text{HH}}$  for small  $k < k^*$  indeed; large- $k$  modes shall agree between wormhole and HH. Briefly recapping, bra-bra wormhole-induced mixing (or entanglement) between scalar fields in separate universes

$$-a_k \phi_1^2(k) + 2b_k \phi_1(k) \phi_2(k) - a_k \phi_2^2(k) \rightarrow -\left(a_k - \frac{b_k^2}{a_k}\right) \phi_1^2(k) \quad (4.7)$$

effectively enhances low- $k$  mode correlations  $\sim 1/a_k^{\text{eff}}$  of  $\phi_1$ , by effectively reducing  $a_k \rightarrow a_k^{\text{eff}} = (a_k^2 - b_k^2)/a_k$ . For this to work,  $b_k < a_k$ , consistently with KSW.

Although we numerically confirmed this low- $k$  enhancement, it is not straightforward to answer why this is compelling. But tracing out the half of dS boundary space is known to induce such an enhancement of low- $k$  correlation in the remaining subsystem [38]. Interactions between two CFTs (that represent each side of a maximally symmetric black hole or each boundary of AdS) can be responsible for the formation of traversable wormholes [39–41]. Thermofield double state is also known to be formed by double trace deformation [42]. ER=EPR is another related conjecture [43, 44]. All these may support why the enhancement of low- $k$  correlation is compelling from interactions between two universes in our solution.

### 4.3 Observable 1 - Comparing longer and shorter inflation

Observable 1 is to compare dS prepared states of different universes with different  $k_{\text{max}}$ , including all modes up to  $k_{\text{max}}$ . Questions for Observable 1: Given the gravitational scale  $S_{\text{dS}}$ , is phase transition and its internal time scale consistent with information physics and chaotic nature of horizon? Here, we attempt to interpret  $k_{\text{max}}$  as some kind of time interval to dS, with aforementioned caution.

Two-point correlations in the full state are calculated by Eq. (4.2) and (4.3). We use  $S_{\text{dS}} = 76$ ,  $\tau_0 = 0.01$  and  $k_{\text{max}} = 150$ ,  $k_{\text{min}} = 0$ ,  $m = 0.3H$ , if not mentioned otherwise.

Above all, Fig. 5 demonstrates the phase transition mechanism. Wormhole effects on  $\langle \phi_k \phi_{-k} \rangle = \text{Tr}[\rho \phi_k \phi_{-k}]$  are visible (as deviations from HH expected results) only for universes with large enough  $k_{\text{max}} \gtrsim 60$ . Once the state  $\rho$  is dominated by wormhole effects

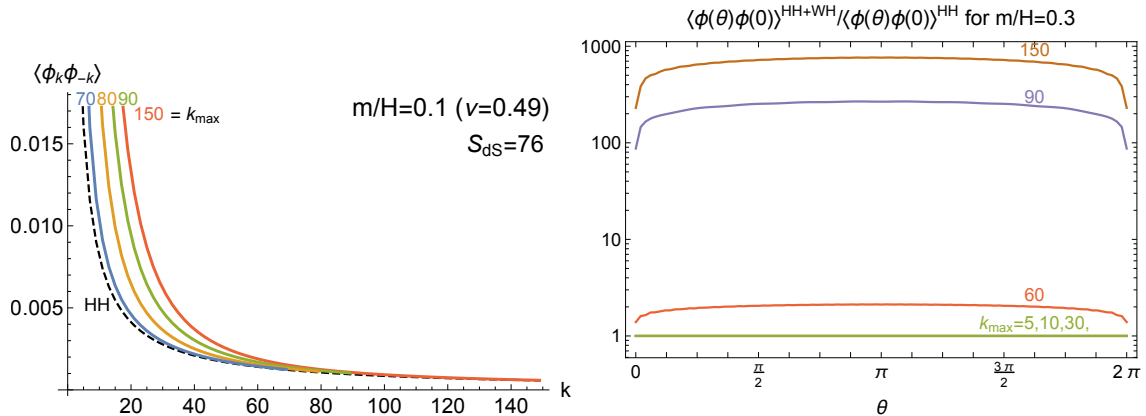


**Figure 5:** Observable 1:  $\langle \phi_k \phi_{-k} \rangle$  (left) and  $\langle \phi(\theta)\phi(0) \rangle$  (right), compared between different  $k_{\text{max}}$ -universes. Wormhole contributions are visible as deviation from HH results (dashed) for  $k_{\text{max}} \gtrsim 60 = k_{\text{max}}^c$ . Small- $k$  or long-range correlations are enhanced.

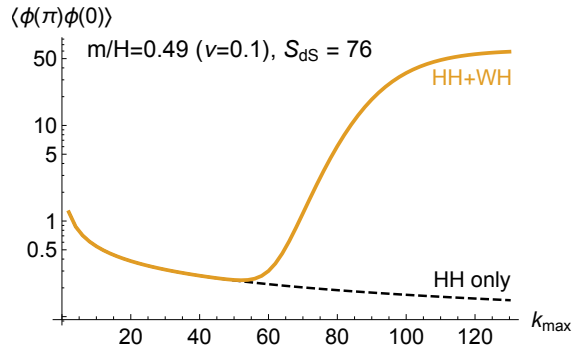
with large  $k_{\text{max}}$ , the deviation is visible predominantly through small- $k$  enhancement of correlation. These are as expected by the mechanism in Sec. 4.2. The fact that wormholes dominate only after long duration of dS stage may be consistent with its possible role of resolving information problem that appears late.

Fig. 5 also makes a consistency check that large- $k$  mode correlations always agree with the leading-order HH results. It is not that the HH term (first term) in Eq. (4.2) dominates the wormhole(WH) term (second term) for large- $k$  correlations, but that  $\text{Im}A_k^{WH} \simeq \text{Im}A_k^{HH}$  for large  $k$  in Eq. (4.6) so that even for WH-dominated states large- $k$  correlation is always that of HH result. This is actually an interesting property of mode functions that satisfy this consistency relation at large  $k$  while allowing wormhole dominant solutions in other regimes.

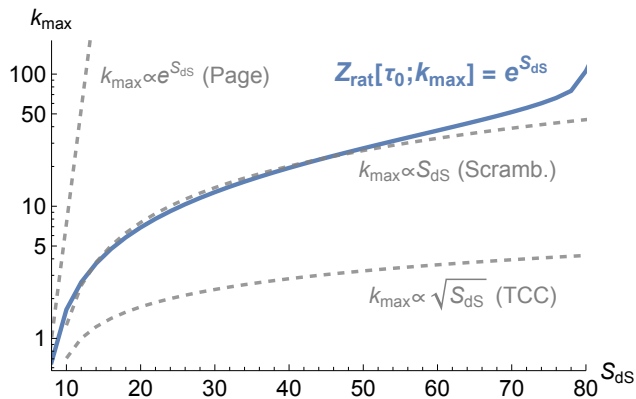
Fig. 5 right panel shows real-space correlations. Unlike scale invariant HH results, WH-dominated spatial correlation is largest between antipodal points  $\theta = \pi$ , while rapidly decreasing for short-distance correlation  $\theta \rightarrow 0, 2\pi$  (but still larger than HH results). This enhancement of long-range correlation was expected if WH solution is to be consistent with KSW. And this might be attributed to wormhole's stereotypical property of entangling widely separated regions of space or shortening a geodesic.

Fig. 6 shows an important result: correlation does not decay indefinitely with time  $k_{\text{max}}$ , but ramps up and plateaus at late time. Similar behavior was found in the AdS-black hole system [10–12], which was largely expected based on the finiteness of Hilbert space [4, 5, 7]. It was also expected in dS [45–47].

As a bonus, Fig. 6 also exhibits quasinormal decays of superhorizon modes (from horizon exit until the end of inflation), shown as the slow decrease of HH results with  $k_{\text{max}}$ . Technically, this effect is incorporated by  $(2\pi/\ell)^{-\Delta_-} = k_{\text{max}}^{-\Delta_-}$  factor in Eq. (3.18). This exponential decay is originated from the exponential expansion of dS universe, but it also suggests that dS is a chaotic quantum system [17, 48, 49].



**Figure 6:** Observable 1: Correlation does not decay forever, but ramps up and reaches a plateau, due to bra-ket wormhole contributions. This feature seems to be consistent with the finiteness of dS horizon entropy. Quasinormal decays of superhorizon modes may reflect the chaotic nature of dS.



**Figure 7:**  $k_{\max}$  at which bra-ket wormhole begins to dominate the total partition function. It turns out to scale as  $\propto S_{\text{dS}}$  ( $Ht \propto \log S_{\text{dS}}$ ) for fixed  $\tau_0 = 0.01$ , reminiscent of the fast scrambling physics. But exact behavior depends on wormhole stabilization mechanism.

The timing of WH dominance in our solution seems to follow the fast scrambling time  $Ht \propto \log S_{\text{dS}}$ , for fixed  $\tau_0 = 0.01$ , as shown in Fig. 7. Different fixed value of  $\tau_0 = 0.001$  also leads to similar behavior (Fig. 14). But true wormhole stabilization shall determine  $\tau_0$  in relation to  $S_{\text{dS}}$ , then this behavior may change. The exact dependence is not known. It is generally expected that distinguishing a mixed state from a pure state in the Hilbert space of dimension  $e^S$  requires to measure  $S$  entropies [13, 14]. This typical time is the Page time  $t \sim \frac{1}{H} \cdot S$ . But for a chaotic system, information can leak out from much earlier time, so called the fast scrambling time  $Ht \sim \log S_{\text{dS}}$  [15, 17]. There are even arguments that dS is a hyperfast scrambling system [16, 50, 51]. Thus, the timing that falls into this range is an interesting result that we do not yet understand why so.

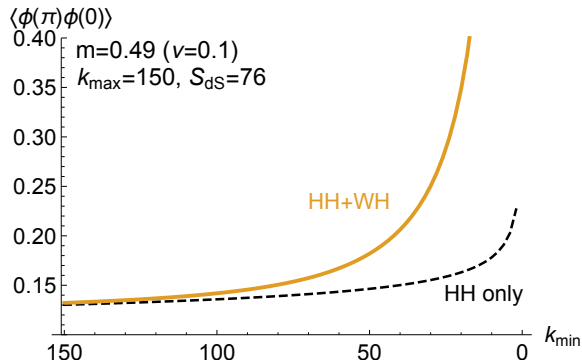


**Figure 8:** Observable 2: Antipodal CMB correlation  $\langle \phi(\pi)\phi(0) \rangle$  as a function of time after reheating,  $k_{\min}$ . Wormhole effects visible only at late times seem to be consistent with the observer’s information viewpoint.

#### 4.4 Observable 2 - CMB-like correlation after reheating

Observable 2 is CMB-like two-point correlations measured by an observer in the flat (or FRW) space after reheating. At each time of measurement (parameterized by  $k_{\min}$ ), we combine only  $k_{\min} \leq k \leq k_{\max}$  modes to calculate real-space correlations in Eq. (4.4).  $k_{\min}$  serves as a time after reheating; decreasing  $k_{\min}$  means time running forward.  $k_{\max}$  is fixed, and the dS prepared state is fixed. This observable is what a post-reheating observer in the given universe would really measure as a function of his cosmological time, via CMB or large scale structures.

Two questions for Observable 2. Is CMB-like observation of dS prepared state consistent with complementarity and resolution of information problem? What are observational features of wormhole dominance, which our cosmological descendants may be able to use to test this idea and understand fundamental physics of dS?

The key result is shown in Fig. 8 that CMB initially looks indistinguishable from HH predictions (Bunch-Davies), but it gradually deviates at late times due to wormhole effects.

Why is this chronological order of CMB observation consistent with information content of the observer? Shortly after reheating, the observer just sees a small amount of information that matches with the HH vacuum, never able to disentangle exponentially suppressed higher topology effects. As he does not gain much information about the fixed state and much uncertainty or possibility remains, the entropy grows. Only after wormhole effects are measured at late times, can he begin to reduce those uncertainties or possibilities, and the entropy decreases. This is also consistent with aforementioned discussion of pure versus mixed state distinction. This chronological phenomenon is very analogous to that of black hole Hawking radiation and the recovery of information(unitarity) after about the Page time.

In a slow-roll inflation, the dS Page time is when the dS horizon entropy is saturated by superhorizon modes generated during inflation. Longer inflation essentially becomes

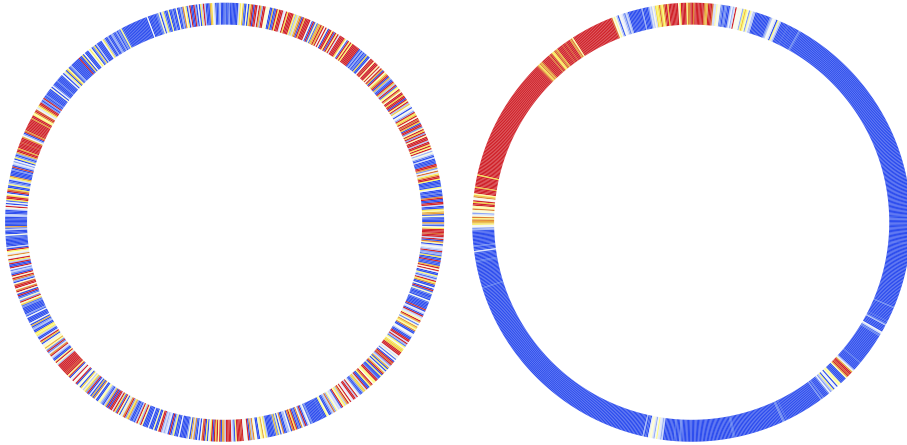


**Figure 9:** Example realization of the CMB field  $\phi(\theta)$ , without(left) and with(right) wormhole contributions.  $k_{\max} = 150, k_{\min} = 0, m = 0.3H, \tau_0 = 0.01, S_{\text{dS}} = 76$ . Enhanced long-range correlations are clear.

an eternal inflation. What happens to the CMB observation? It was argued that density fluctuations generated during the eternal regime are  $\mathcal{O}(1)$  so that no CMB observation after dS Page time can be made, not violating complementarity [14, 52]. Our phase transition that occurs much earlier than the Page time (in Observable 1) may cure or change related physics and observations well before the saturation.

How phase transition occurs while being chronologically consistent is notable, slightly different from that in Observable 1. At early times, only a small number of largest- $k$  modes are observed. They by themselves resemble HH, which was a consistency property. It is not that these largest  $k$ -modes are generated during the HH dominance, rather they are the ones generated at the last stage of dS where wormholes dominate most. But they resemble HH by themselves, even though the fixed state, a sum of the whole modes, is dominated by wormhole effects. As time goes on, smaller  $k$ -modes re-enter, and discernible wormhole contributions gradually appear [13].

Lastly, Fig. 9 and 10 show example late-time CMB distributions on the 1-dimensional space; full results on the right panel is compared with results without wormholes on the left panel. In these sample realizations, field values  $\phi_k$  are random selected according to the Gaussian probability with the width given by  $\langle \phi_k \phi_{-k} \rangle$ . The wormhole effects show up as stronger long-range correlations as expected. This can also be measured as enhanced dipole anisotropy. It is more prominent for light scalars in Fig. 9.

## 5 Summary and Discussion

In this work, we have studied whether bra-ket wormhole saddle solutions to two-point correlators exist and affect in a way (at least qualitatively) consistent with dS information

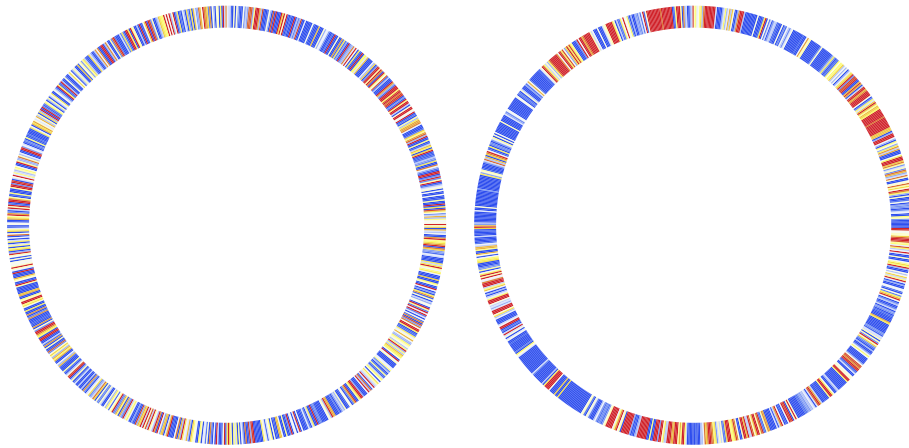


**Figure 10:** Same as Fig. 9, but for heavier  $m = 0.49H$ . Enhancement of long-range correlation is less prominent.

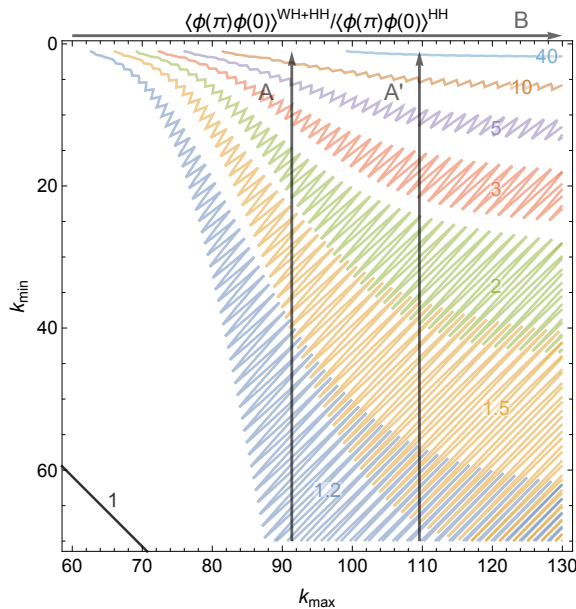


**Figure 11:** Two observables in the full two-dimensional domain  $\{k_{\max}, k_{\min}\}$ . Observable 1, comparing different universes with different  $k_{\max}$ , is along B. Observable 2, measuring CMB of a given universe with time after reheating  $k_{\min}$ , is along A. Also shown are highly oscillating contours of relative wormhole effects, telling its time-dependence in observables.  $S_{\text{dS}} = 76$  and  $\tau_0 = 0.01$ .

problem, in the two-dimensional JT dS plus scalar QFT. Above all, in Sec. 3, we have found a bra-ket wormhole solution at NLO, in addition to a bra-bra and a ket-ket wormholes. To that end, we had to complexify the scale factor, which still satisfies the classicality and relaxed KSW conditions.

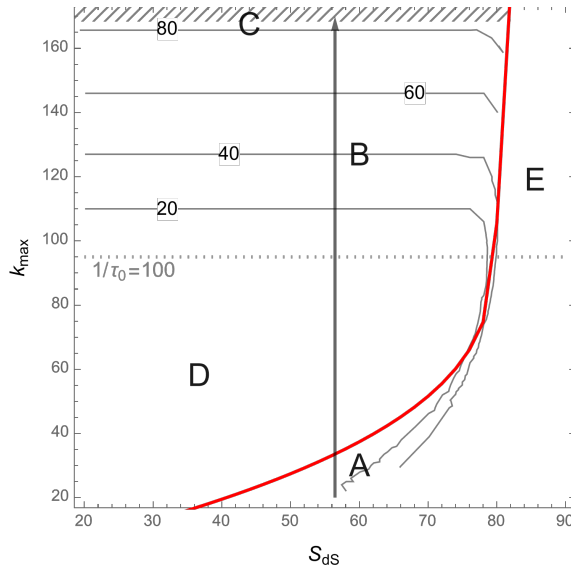


**Figure 12:** Contours of  $k_{\max} - k_{\min}^c$ , the CMB timing that first sees 10% deviation from HH results.  $\tau_0 = 0.01$  determines  $k^* = 1/\tau_0$  (dotted horizontal) above which all modes look like HH states. The wormhole dominance is found in the region above the red boundary  $k_{\max}^c(S_{\text{dS}})$ . Region A: Too short inflation does not need wormhole dominance. B: Long enough inflation with wormhole-dominant state. C, D, E: limitations of our work; see text for detail.

In Sec. 4, we have introduced two correlation observables of the dS prepared state by utilizing two time variables. The relevant parameter spaces they are respectively probing and utilizing are summarized in the full parameter space  $\{k_{\max}, k_{\min}\}$  in Fig. 11. The first observable (along B) compares dS prepared states of different universes, allowing to diagnose the dynamics of phase transition into wormhole dominance. The second observable (along A or A' depending on which  $k_{\max}$ -universe) is basically CMB observable as a function of observer's cosmological time after reheating. Each correlation observable was qualitatively consistent by itself, finding decay-ramp-plateau-type behavior, phase transition at about scrambling time, and consistent chronological order. These were possible due to (1) inflationary exit and re-enter, (2) small- $k$  enhancement of correlations, and (3) phase transition mechanism via competition between mode number and topological suppression. Although results are qualitatively consistent, to really understand them in terms of the entropy context and the chaotic nature of scrambling requires to address following limitations.

**Stabilization of  $\tau_0$  with  $S_{\text{dS}}$ .** An important limitation of this work is that  $\tau_0$  was chosen by hand without relevance to the gravity action (or  $S_{\text{dS}}$ ); even with extra fermions, the saddle point is achieved by the balance between fermions and scalars not involving  $S_{\text{dS}}$ . We first discuss problems with fixed  $\tau_0$ , and possible resolutions, and briefly answer how our qualitative conclusions change with  $\tau_0$  variation.

Fig. 12 shows the contours of  $k_{\max} - k_{\min}^c$ , the difference of  $k_{\max}$  and  $k_{\min}^c$ , which is the CMB timing of revealing wormhole effects in the  $k_{\max}$ -universe. Along the arrow  $A \rightarrow B$ , universes have longer inflation and larger wormhole effects in the partition function. For universes in  $A$ , inflation is too short to have/need wormhole dominance. For universes in  $B$ , our consistent story of wormhole dominance and CMB observation follows. But for universes in  $D$ , where  $k_{\max}^c < k_{\max} < k^* = 1/\tau_0$ , early CMB observation would immediately reveal wormhole effects. One may naively expect that since  $k_{\max}^c$  is determined by interplay of  $\tau_0$  and  $S_{\text{dS}}$ , if  $\tau_0$  is somehow properly determined in relation to  $S_{\text{dS}}$  (so not a fixed quantity) the problem of region  $D$  might be resolved. But actually in our phase transition mechanism,  $k_{\max}^c$  cannot be larger than  $k^* = 1/\tau_0$ . Region  $D$  cannot be avoided in our mechanism.

But the size of region  $D$  may depend on a true wormhole stabilization mechanism. Another missing ingredient might be that due to slow-rolling of the inflaton,  $S_{\text{dS}}$  becomes maximal toward the end of inflation, making wormhole effects relatively smaller there. And these last modes are the ones that will be observed first by CMB observer. It is also an interesting question by itself how to implement slow-rolling in gravitational path integral, or more generally the response of the gravity action to the matter sector which is absent in the JT model. Lastly, one can make an anthropic argument. No advanced observers can exist right after reheating; it always takes some time for universes to evolve to accommodate advanced observers. Notably, this anthropic argument is unique to dS-flat setup, as gravitating and flat regions are timelike separated; black hole observers can exist simultaneously with the black hole.

In universes with very long inflation (region  $C$ ), the CMB reveal of wormhole is also delayed indefinitely. But there shall be some upper limit on this timing, related to the Page time, so this indefinite delay cannot be correct. This region may be related to eternal inflation. But we do not see clear ways how the fact that inflation is eternal causes problems in this work, and we leave investigation for future works.

In universes in  $E$ , right to the red boundary,  $S_{\text{dS}}$  is too large to allow phase transition for any large  $k_{\max}$ . This might also be due to fixed  $\tau_0$  independently of  $S_{\text{dS}}$  as well as missing higher-order wormhole saddles and off-shell wormholes [37, 53]. For example, if  $\tau_0$  saddle were smaller for larger  $S_{\text{dS}}$ , the red boundary would have moved to the right bottom.

We wrap up this issue by asking: under variation of  $\tau_0$ , how would our results change? In Appendix C, we briefly show that for certain choices of parameters  $\{S_{\text{dS}}, \tau_0, k_{\max}\}$  related by some scaling, the shape of plots remain similar and our qualitative conclusions still hold. This is especially true for results with fixed  $S_{\text{dS}} = 76$ . But for the timing result as a function of  $S_{\text{dS}}$  do depend on exact stabilization mechanism.

**Implications.** Our explicit wormhole solution may shed some light on dS-CFT correspondence. The expected asymptotic behavior of the scalar field in Eq. (3.6)

$$\Phi \sim \phi e^{-\Delta_- t} + \mathcal{O} e^{-\Delta_+ t} \simeq \phi (-\eta)^{\Delta_-} + \mathcal{O} (-\eta)^{\Delta_+} \quad (5.1)$$

is confirmed in our explicit solution of wormhole too. Written in terms of the conformal time  $\eta = -e^{-t}$ , this makes it clear that the conformal invariance of 2d-scalar  $\Phi$  implies 1d-CFT transformation of  $\phi$  and  $\mathcal{O}$  with conformal dimension  $\Delta_-$  and  $\Delta_+$ , respectively. The resulting CFT correlation  $\langle \phi(x)\phi(x') \rangle \sim |x - x'|^{-2\Delta_-}$  is reproduced exactly by the HH wavefunction, which is a well-known support of the conjecture of dS-CFT correspondence [54, 55]. In our wormhole solution, this correlation was modified even though the asymptotic form and the conformal dimensions  $\Delta_{\pm}$  remain unmodified. It suggests that the corresponding CFTs may be modified by interactions between same kind of operators. This is reminiscent of how traversable wormholes in AdS is generated by double-trace deformation that couples the two boundary CFTs [39–41] preparing the entangled thermofield double state [42]. We leave detailed check of correspondence in this solution for future work.

Another implication of modified two-point functions is on the stochastic description of inflation [56, 57]. This description is based on the local interplay of deterministic classical rolling (drift) of inflaton( $\Phi$ ) and random fluctuation (diffusion) from two-point function. Instead of scale invariant diffusion  $\sim H/2\pi$  from the HH two-point function, our wormhole solution will lead to scale-dependent diffusion, via enhanced long-wavelength correlation at early stage of slow-rolling. This may modify the global probability distribution of the inflaton field value, potentially affecting ‘natural’ outcomes of inflaton-dependent ‘inputs’ to the big-bang universe [58, 59].

## Acknowledgments

We thank Hyung Do Kim, Seok Kim, Jiwoo Park, Dong-han Yeom, Junggi Yoon for valuable comments and encouragement. We are supported by Grant Korea NRF2019R1C1C1010050 and RS-2024-00342093.

## A Scalar field solutions and correlators

### A.1 Hartle-Hawking

We first analyse the scalar field on the Hartle-Hawking geometry with metric

$$ds^2 = -dt^2 + \cosh^2 t d\theta^2. \quad (\text{A.1})$$

The governing equation for the scalar field  $\Phi_k(t)$  of mass  $m$  is written by

$$\partial_t^2 \Phi_k(t) + \tanh t \partial_t \Phi_k(t) + \left( \frac{k^2}{\cosh^2 t} + m^2 \right) \Phi_k(t) = 0. \quad (\text{A.2})$$

We impose boundary conditions at a late-time cutoff surface,

$$\Phi_k(t_\epsilon) = \phi(k), \quad (\text{A.3})$$

with  $t_\epsilon = \log(2/\epsilon)$ . The solution is required to be regular on the full geometry, including the Euclidean cap. Regularity at the pole of the Euclidean hemisphere removes the negative-frequency modes and prepares the Hartle–Hawking state, which coincides with the Bunch–Davies vacuum in the Lorentzian regime.

The resulting solution can be written as

$$\Phi_k(t) = \phi(k) \frac{u_k(t)}{u_k(t_\epsilon)}, \quad u_k(t) = \frac{i^{\Delta_- - \pi}}{2^\nu \Gamma(\nu)} (\tanh^2 t - 1)^{1/4} \left( P_{k-1/2}^\nu(\tanh t) - \frac{2i}{\pi} Q_{k-1/2}^\nu(\tanh t) \right), \quad (\text{A.4})$$

where  $u_k(t)$  is the linear combination of associated Legendre functions that is regular on the Euclidean cap. For  $t_\epsilon \gg 1$ , its asymptotic behavior is

$$u_k(t_\epsilon) = \left[ \epsilon^{\Delta_-} + i^{2\nu} \frac{\Gamma(-\nu)}{4^\nu \Gamma(\nu)} \frac{\Gamma(\Delta_+ + k)}{\Gamma(\Delta_- + k)} \epsilon^{\Delta_+} \right]. \quad (\text{A.5})$$

In terms of the boundary value  $\phi$ , the on-shell action is

$$\begin{aligned} iS[g_{\text{cl}}, \Phi_{\text{cl}}] &= \frac{i}{2} \int d\theta a(t) \Phi_{\text{cl}}(t, \theta) \partial_t \Phi_{\text{cl}}(t, \theta) \Big|_{t=t_\epsilon} \\ &= i\pi \sum_k \phi(k) \phi(-k) \frac{1}{\epsilon} \frac{\partial_t u(t)}{u(t_\epsilon)} \Big|_{t=t_\epsilon} \\ &= -i\pi \sum_k \phi(k) \phi(-k) \frac{1}{\epsilon} \left[ \Delta_- + 2\nu i^{2\nu} \frac{\Gamma(-\nu)}{4^\nu \Gamma(\nu)} \frac{\Gamma(\Delta_+ + k)}{\Gamma(\Delta_- + k)} \epsilon^{2\nu} + \dots \right]. \end{aligned} \quad (\text{A.6})$$

The first term in the square bracket does not contribute to the observables since it cancels upon taking the modulus squared. The imaginary part of the second term is the leading one in the computation with the factor,  $\epsilon^{-1+2\nu} = \left(\frac{2\pi}{\ell}\right)^{-1+2\nu}$ . This reproduces the standard Bunch–Davies two-point function.

The density matrix for the boundary configurations is then

$$\rho(\phi) \propto |e^{iS}|^2 = \exp \left[ - \sum_k \left( \frac{2\pi}{\ell} \right)^{-2\Delta_-} \frac{4\pi^2}{4^\nu \Gamma[\nu]^2} \frac{\Gamma(\Delta_+ + k)}{\Gamma(\Delta_- + k)} \phi(k) \phi(-k) \right]. \quad (\text{A.7})$$

The two-point function follows from a Gaussian integral over the boundary fields,

$$\int D\phi \phi(k) \phi(-k) \rho(\phi) = \left( \frac{2\pi}{\ell} \right)^{2\Delta_-} \frac{4^\nu \Gamma[\nu]^2}{4\pi^2} \frac{\Gamma(\Delta_- + k)}{\Gamma(\Delta_+ + k)}, \quad (\text{A.8})$$

which matches the expected Bunch–Davies correlator, reproducing the results in [34] in the global coordinate.

In the gravity side, the bulk gravitational action reduces to a boundary term, parametrized by the Schwarzian modes  $\theta$  [34, 60].

$$S_{\text{grav}} = \frac{\varphi_0}{4G_2} \chi + \frac{\varphi_r}{8\pi G_2} \int_0^{2\pi} d\theta \left( \{f(\theta), \theta\} + \frac{f'(\theta)^2}{2} \right), \quad (\text{A.9})$$

where  $\chi = -i$  for Hartle-Hawking and  $f(\theta)$  parametrizes the boundary curve. The Schwarzian derivative is defined as

$$\{f(x), x\} \equiv \frac{f''(x)^2}{2 f'(x)^3} - \frac{f'''(x)}{3 f'(x)^2}. \quad (\text{A.10})$$

The topological term in Eq. (A.9) contributes a factor  $\exp(S_{dS})$ , making the Hartle-Hawking contribution dominant over higher-genus saddles, while the Schwarzian term vanishes upon setting  $f(\theta) = \theta$  before squaring the wave function to extract probabilities.

## A.2 Two-boundary wormhole

To capture the NLO contributions from wormhole saddles, we now solve the scalar equation on a different background. A wormhole scale factor is

$$a(t) = \frac{1}{2} (e^t + e^{i\tau_0 - t}). \quad (\text{A.11})$$

The EoM for the scalar field on this geometry becomes

$$\partial_t^2 \Phi_k(t) + \tanh(t - i\tau_0/2) \partial_t \Phi_k(t) + \left( \frac{k^2}{e^{i\tau_0} \cosh^2(t - i\tau_0/2)} + m^2 \right) \Phi_k(t) = 0. \quad (\text{A.12})$$

A general solution can be written as

$$v_k(t) = e^{t(\frac{1}{2} - \nu) + i\nu\tau_0} (e^{2t} + e^{i\tau_0})^{-\tilde{k}} \left[ C_2 {}_2F_1\left(\frac{1}{2} - \tilde{k}, \frac{1}{2} - \tilde{k} - \nu, 1 - \nu, -e^{2t - i\tau_0}\right) + C_1 e^{2\nu t + i(2\pi - \tau_0)\nu} {}_2F_1\left(\frac{1}{2} - \tilde{k}, \frac{1}{2} - \tilde{k} + \nu, 1 + \nu, -e^{2t - i\tau_0}\right) \right], \quad (\text{A.13})$$

where we defined  $\tilde{k} = e^{-i\tau_0/2} k$ .

We impose boundary conditions at the two asymptotic boundaries, located at  $t = t_\epsilon, -t_\epsilon + i\tau_0$

$$\Phi_k(t_\epsilon) = \phi_1(k), \quad \Phi_k(-t_\epsilon + i\tau_0) = \phi_2(k). \quad (\text{A.14})$$

These conditions fix the coefficients  $C_1, C_2$  as

$$C_1 = \frac{e^{-i\pi\nu} 2^{\Delta_-} e^{-\frac{i}{2}(1-2\tilde{k})\tau_0} \Gamma\left(\frac{1}{2} - \tilde{k} + \nu\right) \Gamma\left(\frac{1}{2} + \tilde{k} + \nu\right)}{\Gamma(\nu) \Gamma(1 + \nu)} \left[ \phi_1 - \phi_2 \cos(\tilde{k}\pi) \csc(\pi\nu) \right], \quad (\text{A.15})$$

$$C_2 = e^{i\pi\nu} 2^{\Delta_-} e^{-\frac{i}{2}(1-2\tilde{k})\tau_0} \phi_2. \quad (\text{A.16})$$

The field is constructed by the combination of

$$\Phi_k(t) = \phi_1(k) \frac{v_k(t)}{v_k(t_\epsilon)} = \phi_2(k) \frac{v_k(t)}{v_k(-t_\epsilon + i\tau_0)}. \quad (\text{A.17})$$

Employing the asymptotic form of the  $v(t) \simeq \phi a(t)^{-\Delta_-} + \mathcal{O} a(t)^{-\Delta_+}$ , the boundary values of the fields and its time derivatives are

$$\Phi_k(t_\epsilon) = \phi_1(k), \quad (\text{A.18})$$

$$\dot{\Phi}_k(t_\epsilon) = -2\nu \mathcal{O}_1(k) \epsilon^{2\nu}. \quad (\text{A.19})$$

At the other boundary, the expressions are analogous with 1 and 2 interchanged.  $\mathcal{O}_{1,2} = \tilde{a}\phi_{1,2} + \tilde{b}\phi_{2,1}$  can be obtained by expanding  $u_k(t)$  near the boundary,

$$\tilde{a}_k = - \frac{4^{\Delta_-} e^{i\nu\tau_0} \pi^2 \cos(\tilde{k}\pi) \csc(\pi\nu)}{(\cos(2\tilde{k}\pi) + \cos(2\pi\nu)) \Gamma\left(\frac{1}{2} - \tilde{k} - \nu\right) \Gamma\left(\frac{1}{2} + \tilde{k} - \nu\right) \Gamma(\nu) \Gamma(1 + \nu)}, \quad (\text{A.20})$$

$$\tilde{b}_k = \frac{4^{\Delta_-} e^{i\nu\tau_0} \pi^2}{(\cos(2\tilde{k}\pi) + \cos(2\pi\nu)) \Gamma\left(\frac{1}{2} - \tilde{k} - \nu\right) \Gamma\left(\frac{1}{2} + \tilde{k} - \nu\right) \Gamma(\nu) \Gamma(1 + \nu)}. \quad (\text{A.21})$$

The on-shell action receives contributions from both boundaries,

$$S = -2\nu\pi \sum_k (\phi_1(-k) \mathcal{O}_1(k) + \phi_2(-k) \mathcal{O}_2(k)) \quad (\text{A.22})$$

$$= -2\nu\pi \sum_k [\tilde{a}_k |\phi_1(k)|^2 + \tilde{b}_k [\phi_1(k)\phi_2(-k) + \text{c.c.}] + \tilde{a}_k |\phi_2(k)|^2]. \quad (\text{A.23})$$

As discussed above, the imaginary parts of the coefficients  $\tilde{a}_k$  and  $\tilde{b}_k$  determine the induced boundary correlators. The complex squaring of the path integral and the subsequent tracing-out procedure are carried out in Sec. 3.3, where we construct the physical density matrix relevant for observables.

## B Stabilizing bra-ket wormhole by extra fermions

To stabilize the wormhole, we can introduce the additional degrees of freedom for a fermion field whose action [61, 62] is

$$\mathcal{S} = -\frac{1}{2} \int d^2x \sqrt{-g} \left( \frac{i}{2} \bar{\psi} \overleftrightarrow{\mathcal{D}} \psi + m \bar{\psi} \psi \right) + \frac{1}{2} \int d\theta \sqrt{h} \bar{\psi} \gamma^0 \psi. \quad (\text{B.1})$$

The covariant Dirac operator in dS<sub>2</sub> is defined using the zweibein  $e_a^\mu$  as  $\mathcal{D} = \gamma^\mu D_\mu = \gamma^a e_a^\mu (\partial_\mu + \frac{1}{4} \omega_\mu^{bc} \gamma_{bc})$  where  $\omega_\mu^{bc}$  is the spin connection and  $\gamma_{bc} = \frac{1}{2} [\gamma_b, \gamma_c]$ . The boundary term is included in order to render the variational problem well-posed and guarantee  $\delta S = 0$ . The EoM for the two-component fermion field,  $\psi = (u, v)^t$  is written as

$$\left( \partial_t + \frac{\dot{a}(t)}{2a(t)} - \frac{ik}{a(t)} \right) u + mv = 0, \quad (\text{B.2})$$

$$\left( \partial_t + \frac{\dot{a}(t)}{2a(t)} + \frac{ik}{a(t)} \right) v + mu = 0, \quad (\text{B.3})$$

working in the metric of  $ds^2 = -dt^2 + a(t)^2 d\theta^2$ . They reduce to the two coupled 2nd ODEs such as

$$\partial_t^2 u(t, k) + \frac{\dot{a}(t)}{a(t)} \partial_t u(t, k) + \left[ -m^2 + \frac{\ddot{a}(t)}{2a(t)} + \left( \frac{k}{a(t)} + i \frac{\dot{a}(t)}{2a(t)} \right)^2 \right] u(t, k) = 0, \quad (\text{B.4})$$

$$v(t, k) = -\frac{1}{m} \left( \partial_t + \frac{\dot{a}(t)}{2a(t)} - \frac{ik}{a(t)} \right) u(t, k), \quad (\text{B.5})$$

where  $a(t) = e^{i\tau_0/2} \cosh(t - i\frac{\tau_0}{2})$  for the wormhole geometry we find in Sec. 3.2. After solving the EoM, one can expand the field near the asymptotic boundaries as done in the scalar field

$$\psi(t, k) \simeq \chi_0(k) e^{-\left(\frac{1}{2}-m\right)t} \hat{\psi}_+ + \mathcal{O}(k) e^{-\left(\frac{1}{2}+m\right)t} \hat{\psi}_-, \quad (\text{B.6})$$

$$\bar{\psi}(t, k) \simeq \bar{\chi}_0(k) e^{-\left(\frac{1}{2}-m\right)t} \hat{\psi}_- + \bar{\mathcal{O}}(k) e^{-\left(\frac{1}{2}+m\right)t} \hat{\psi}_+. \quad (\text{B.7})$$

The spinors are defined by  $\hat{\psi}_\pm = (1, \pm 1)^t$  with the boundary field value of  $\chi_0$ . The boundary term in the action is evaluated and the remaining contribution of LO in the limit of  $t \rightarrow \infty$  is

$$\frac{1}{2} \int d\theta a(t) \bar{\psi}(t, \theta) \gamma^0 \psi(t, \theta) \Big|_{t \rightarrow \infty} = i \sum_k [\bar{\chi}_0(-k) \mathcal{O}(k) - \bar{\mathcal{O}}(-k) \chi_0(k)]. \quad (\text{B.8})$$

In the wormhole geometry, the field has the boundary values of  $\chi_{1,2}$  at each boundary. The quantities of  $\mathcal{O}$  are written schematically by  $\mathcal{O}_1 = a\chi_1 + b\chi_2$ ,  $\mathcal{O}_2 = b\chi_1 - a\chi_2$ . The boundary action would read

$$\begin{aligned} iS_b &= \frac{i}{2} \left( \int d\theta a(t) \bar{\psi}_1(t, \theta) \gamma^0 \psi_1(t, \theta) - \int d\theta a(t) \bar{\psi}_2(t, \theta) \gamma^0 \psi_2(t, \theta) \right) \\ &= -2 \sum_{k \in \mathbb{Z} + \frac{1}{2}} [a_k \bar{\chi}_2(-k) \chi_2(k) - b_k (\bar{\chi}_2(-k) \chi_1(k) + \chi_2(k) \bar{\chi}_1(-k)) + a_k \bar{\chi}_1(-k) \chi_1(k)]. \end{aligned} \quad (\text{B.9})$$

The  $\chi_2$  are integrated out as they are in the unobservable boundary and it provides the modified action yielding the probability and the correlator,

$$\rho[\chi_1, \chi_1] = \mathcal{N} \int D\bar{\chi}_2 D\chi_2 \exp[i(S_b - S_b^*)] \sim \prod_{k \in \mathbb{Z} + \frac{1}{2}} \exp \left[ -4 \left( \text{Re} a_k + \frac{(\text{Im} b_k)^2}{\text{Re} a_k} \right) \bar{\chi}_1(-k) \chi_1(k) \right]. \quad (\text{B.10})$$

The fermionic contribution to the partition function depends on the product of the quadratic coefficients, rather than on their inverse. As a consistency, the coefficient of  $\bar{\chi}\chi$  has the correction sign in order that the partition function is positive and has the appropriate physical meaning.

This coefficient vanishes linearly in  $\tau_0 \rightarrow 0$ , and therefore compensates the  $1/\tau_0$ -type divergence arising from the scalar sector. If the particle spectrum consists of two scalar

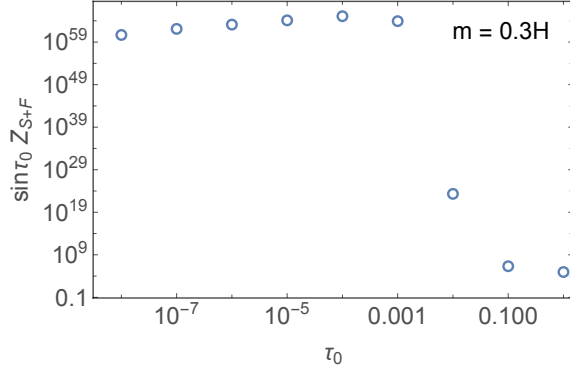


**Figure 13:** This figure shows the  $Z_{rat}$ , including the two scalar fields and a spinor field with  $k_{\max} = 200$ . Fermions and scalars compete to yield nonzero finite saddle point of  $\tau_0$ , typically  $\sim 10^{-3} - 10^{-2}$  for the given parameters of the universe.

fields and one fermion, the combined matter partition function can be written schematically as

$$Z^{WH} = \int D\phi D\bar{\chi} D\chi |\Psi[\phi, \chi]|^2 = \prod_k \frac{1}{\text{Im}A_k^{\text{scalar}}} \cdot \left( \text{Re}a_k + \frac{(\text{Im}b_k)^2}{\text{Re}a_k} \right), \quad (\text{B.11})$$

where  $A_k^{\text{scalar}}$  is the scalar kernel which vanishes linearly in  $\tau_0$ . One can check that the total integrand remains finite even in the limit of  $\tau_0 \rightarrow 0$ .

We can then compute the ratio  $Z_{S+F} = Z^{WH}(\tau_0)/Z^{HH}$  for this combined matter spectrum ( $S+F$ ). As shown in Fig. 13, the resulting partition function is finite throughout the range of  $\tau_0$ , and the dominant contribution comes from a saddle at nonzero  $\tau_0$ .

### C $\tau_0$ dependence

A true wormhole stabilization mechanism will have to determine  $\tau_0$  in relation to  $S_{\text{dS}}$ . Without having a solid mechanism, we briefly vary  $\tau_0$  and see how our results change.

Fig. 14 shows the results for 10 times smaller  $\tau_0 = 0.001$ . They correspond to Fig. 7, 5, 6, and 8. They show similar behaviors if correspondingly larger  $S_{\text{dS}}$  and  $k_{\max}$  are chosen. But the timing plot as a function of  $S_{\text{dS}}$  shall depend on exact stabilization mechanism yielding a relation between  $\tau_0$  and  $S_{\text{dS}}$ .

### D Suppression of contributions from multiple wormholes

We argue that the tracing-out procedure allows multiboundary wormholes to contribute to two-boundary quantities in the path integral. In particular, one may consider the possibility that geometries with more than two boundaries can be traced out to yield an two-boundary quantity. In this appendix we analyze this possibility and conclude that their contributions are suppressed by the number of wormhole geometries.

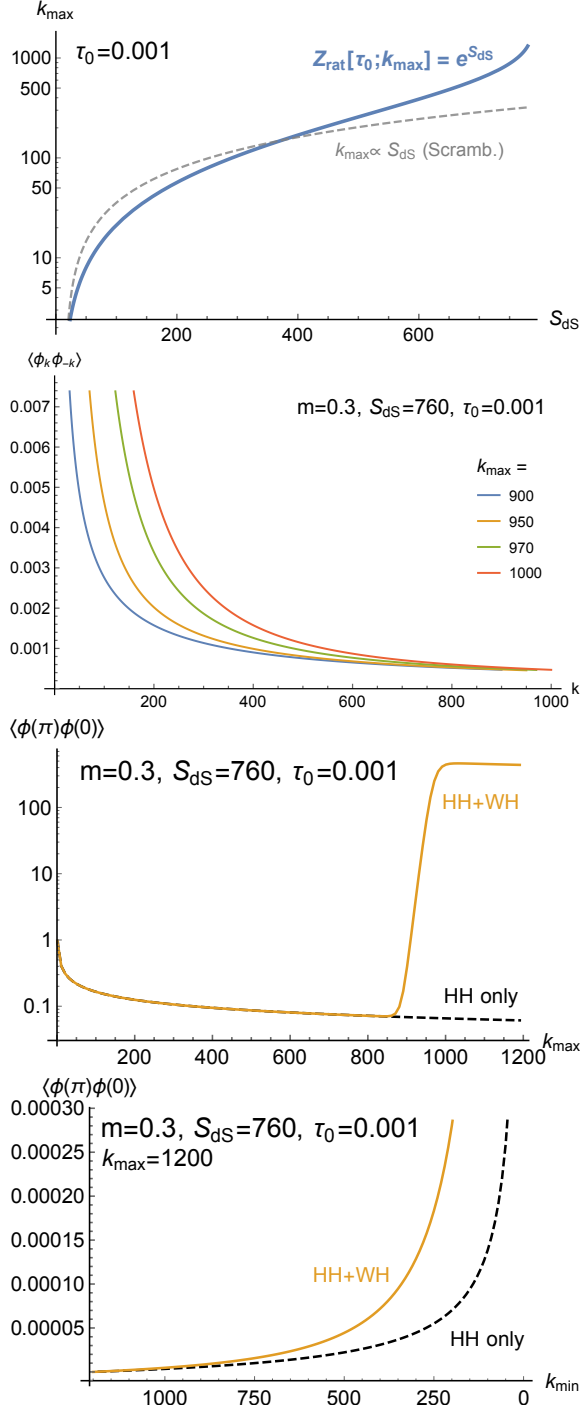


**Figure 14:** For a smaller fixed value of  $\tau_0 = 0.001$ , similar behaviors are obtained if correspondingly larger  $S_{\text{dS}}$  and  $k_{\max}$  are chosen. But the timing behavior further depends on exact wormhole stabilization mechanism, yielding a relation between  $\tau_0$  and  $S_{\text{dS}}$ .

We can connect more than two wormholes and trace them out systematically to obtain the wave functional. The resulting wormhole geometry produces an amplitude of the very

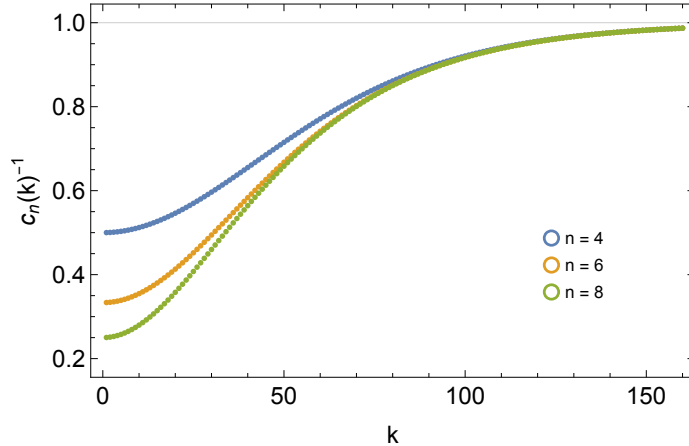


**Figure 15:** Inverse ratio factor  $c_n(k)^{-1}$  to the leading coefficients for traced multi-wormholes. The three colored curves correspond to an increasing number of traced wormholes for  $n = 4, 6, 8$ . For small  $k$  the factor lies well below 1, indicating a strong suppression when all  $c(k)^{-1}$  are multiplied.

schematic form

$$iS[\phi_1, \phi_2] = -a\phi_1^2 + 2b\phi_1\phi_2 - a\phi_2^2. \quad (\text{D.1})$$

Here,  $\phi_{1,2}$  are the boundary values of the field on the two boundaries the wormhole saddle connects. For the main results' case ( $n = 2$ ), we have

$$\mathcal{N} \int \mathcal{D}\phi_0 \exp[iS[\phi_0, \phi] - iS^*[\phi_0, \phi]] \sim \exp(-\mathcal{I}\phi^2), \quad (\text{D.2})$$

where  $\mathcal{I} \equiv (\alpha^2 - \beta^2)/\alpha$ . The notations are same with ones in the 3.3. The  $n = 4$  contribution is obtained by tracing out three boundary values ( $\phi_{0,1,2}$ ) and is evaluated as

$$\mathcal{N} \int \mathcal{D}\phi_0 \mathcal{D}\phi_1 \mathcal{D}\phi_2 \exp[iS[\phi_0, \phi_1] - iS^*[\phi_0, \phi_2] + iS[\phi_2, \phi] - iS^*[\phi_1, \phi]] \sim \exp(-\mathcal{I}c_{n=4}\phi^2). \quad (\text{D.3})$$

Here  $c_n$  denotes the ratio of the  $n$ -wormhole contribution to that of the leading bra-ket wormhole. Tracing out four wormholes therefore yields a probability distribution only for  $\phi$ . Comparing the various contributions, the partition function obtained after integrating over  $\phi$  becomes

$$\int \exp\left[-\sum_k \mathcal{I}(k) c_n(k) \phi_k^2\right] = \prod_k \sqrt{\frac{\pi}{c_n(k) \mathcal{I}(k)}} = \left(\prod_k \frac{1}{\sqrt{c_n(k)}}\right) Z_{n=2}. \quad (\text{D.4})$$

Hence the overall normalization from  $n$  wormholes is suppressed by the product of factors  $1/\sqrt{c_n(k)}$ , as shown in Fig. 15. Each factor satisfies  $0 < c_n(k) < 1$  and decreases further as  $n$  becomes large or  $\tau_0$  becomes smaller. It can be probed that the  $c_n(k=0) \propto n$  by the mathematical induction. Consequently, the more wormholes are traced out, the more strongly their contributions are suppressed in the path integral.

## References

- [1] G. W. Gibbons and S. W. Hawking, *Cosmological Event Horizons, Thermodynamics, and Particle Creation*, *Phys. Rev. D* **15** (1977) 2738–2751.
- [2] J. D. Bekenstein, *Black holes and entropy*, *Phys. Rev. D* **7** (1973) 2333–2346.
- [3] S. W. Hawking, *Particle Creation by Black Holes*, *Commun. Math. Phys.* **43** (1975) 199–220. [Erratum: *Commun.Math.Phys.* 46, 206 (1976)].
- [4] E. Witten, *Quantum gravity in de Sitter space*, in *Strings 2001: International Conference*, 6, 2001. [hep-th/0106109](#).
- [5] N. Goheer, M. Kleban, and L. Susskind, *The Trouble with de Sitter space*, *JHEP* **07** (2003) 056, [[hep-th/0212209](#)].
- [6] M. K. Parikh and E. P. Verlinde, *De Sitter holography with a finite number of states*, *JHEP* **01** (2005) 054, [[hep-th/0410227](#)].
- [7] J. M. Maldacena, *Eternal black holes in anti-de Sitter*, *JHEP* **04** (2003) 021, [[hep-th/0106112](#)].
- [8] J. B. Hartle and S. W. Hawking, *Wave Function of the Universe*, *Phys. Rev. D* **28** (1983) 2960–2975.
- [9] A. Castro and A. Maloney, *The Wave Function of Quantum de Sitter*, *JHEP* **11** (2012) 096, [[arXiv:1209.5757](#)].
- [10] P. Saad, S. H. Shenker, and D. Stanford, *A semiclassical ramp in SYK and in gravity*, [arXiv:1806.06840](#).
- [11] P. Saad, S. H. Shenker, and D. Stanford, *JT gravity as a matrix integral*, [arXiv:1903.11115](#).
- [12] P. Saad, *Late Time Correlation Functions, Baby Universes, and ETH in JT Gravity*, [arXiv:1910.10311](#).
- [13] D. N. Page, *Information in black hole radiation*, *Phys. Rev. Lett.* **71** (1993) 3743–3746, [[hep-th/9306083](#)].
- [14] N. Arkani-Hamed, S. Dubovsky, A. Nicolis, E. Trincherini, and G. Villadoro, *A Measure of de Sitter entropy and eternal inflation*, *JHEP* **05** (2007) 055, [[arXiv:0704.1814](#)].
- [15] P. Hayden and J. Preskill, *Black holes as mirrors: Quantum information in random subsystems*, *JHEP* **09** (2007) 120, [[arXiv:0708.4025](#)].
- [16] L. Susskind, *Addendum to Fast Scramblers*, [arXiv:1101.6048](#).
- [17] J. Maldacena, S. H. Shenker, and D. Stanford, *A bound on chaos*, *JHEP* **08** (2016) 106, [[arXiv:1503.01409](#)].
- [18] J. Preskill, *Do black holes destroy information?*, in *International Symposium on Black holes, Membranes, Wormholes and Superstrings*, 1, 1992. [hep-th/9209058](#).
- [19] A. Almheiri, T. Hartman, J. Maldacena, E. Shaghoulian, and A. Tajdini, *The entropy of Hawking radiation*, *Rev. Mod. Phys.* **93** (2021), no. 3 035002, [[arXiv:2006.06872](#)].
- [20] G. Penington, S. H. Shenker, D. Stanford, and Z. Yang, *Replica wormholes and the black hole interior*, *JHEP* **03** (2022) 205, [[arXiv:1911.11977](#)].
- [21] Y. Chen, V. Gorbenko, and J. Maldacena, *Bra-ket wormholes in gravitationally prepared states*, *JHEP* **02** (2021) 009, [[arXiv:2007.16091](#)].

- [22] A. Fumagalli, V. Gorbenko, and J. Kames-King, *De Sitter Bra-Ket wormholes*, *JHEP* **05** (2025) 074, [[arXiv:2408.08351](#)].
- [23] R. Jackiw, *Lower Dimensional Gravity*, *Nucl. Phys. B* **252** (1985) 343–356.
- [24] C. Teitelboim, *Gravitation and Hamiltonian Structure in Two Space-Time Dimensions*, *Phys. Lett. B* **126** (1983) 41–45.
- [25] J. J. Halliwell and J. B. Hartle, *Integration Contours for the No Boundary Wave Function of the Universe*, *Phys. Rev. D* **41** (1990) 1815.
- [26] J. B. Hartle, S. W. Hawking, and T. Hertog, *The Classical Universes of the No-Boundary Quantum State*, *Phys. Rev. D* **77** (2008) 123537, [[arXiv:0803.1663](#)].
- [27] D.-i. Hwang, S. A. Kim, and D.-h. Yeom, *No-boundary wave function for two-field inflation*, *Class. Quant. Grav.* **32** (2015), no. 11 115006, [[arXiv:1404.2800](#)].
- [28] M. Kontsevich and G. Segal, *Wick Rotation and the Positivity of Energy in Quantum Field Theory*, *Quart. J. Math. Oxford Ser.* **72** (2021), no. 1-2 673–699, [[arXiv:2105.10161](#)].
- [29] E. Witten, *A Note On Complex Spacetime Metrics*, [arXiv:2111.06514](#).
- [30] R. Bousso, *Positive vacuum energy and the N bound*, *JHEP* **11** (2000) 038, [[hep-th/0010252](#)].
- [31] J. Maldacena and G. L. Pimentel, *Entanglement entropy in de Sitter space*, *JHEP* **02** (2013) 038, [[arXiv:1210.7244](#)].
- [32] D. Teresi, *Islands and the de Sitter entropy bound*, *JHEP* **10** (2022) 179, [[arXiv:2112.03922](#)].
- [33] D. Stanford and E. Witten, *Fermionic Localization of the Schwarzian Theory*, *JHEP* **10** (2017) 008, [[arXiv:1703.04612](#)].
- [34] J. Maldacena, G. J. Turiaci, and Z. Yang, *Two dimensional Nearly de Sitter gravity*, *JHEP* **01** (2021) 139, [[arXiv:1904.01911](#)].
- [35] T. Anous, J. Kruthoff, and R. Mahajan, *Density matrices in quantum gravity*, *SciPost Phys.* **9** (2020), no. 4 045, [[arXiv:2006.17000](#)].
- [36] A. Milekhin and A. Tajdini, *Bra-ket wormholes and Casimir entropy*, [arXiv:2212.08246](#).
- [37] S. Jung, S. Kim, J. Park, and S. Song, “Random matrix product state models of gravitationally prepared states.” in preparation, 2025.
- [38] S. Kanno, *Impact of quantum entanglement on spectrum of cosmological fluctuations*, *JCAP* **07** (2014) 029, [[arXiv:1405.7793](#)].
- [39] P. Gao, D. L. Jafferis, and A. C. Wall, *Traversable Wormholes via a Double Trace Deformation*, *JHEP* **12** (2017) 151, [[arXiv:1608.05687](#)].
- [40] J. Maldacena, D. Stanford, and Z. Yang, *Diving into traversable wormholes*, *Fortsch. Phys.* **65** (2017), no. 5 1700034, [[arXiv:1704.05333](#)].
- [41] J. Maldacena and X.-L. Qi, *Eternal traversable wormhole*, [arXiv:1804.00491](#).
- [42] W. Cottrell, B. Freivogel, D. M. Hofman, and S. F. Lokhande, *How to Build the Thermofield Double State*, *JHEP* **02** (2019) 058, [[arXiv:1811.11528](#)].
- [43] J. Maldacena and L. Susskind, *Cool horizons for entangled black holes*, *Fortsch. Phys.* **61** (2013) 781–811, [[arXiv:1306.0533](#)].

- [44] L. Susskind, *ER=EPR, GHZ, and the consistency of quantum measurements*, *Fortsch. Phys.* **64** (2016) 72–83, [[arXiv:1412.8483](#)].
- [45] L. Aalsma, M. M. Faruk, J. P. van der Schaar, M. R. Visser, and J. de Witte, *Late-time correlators and complex geodesics in de Sitter space*, *SciPost Phys.* **15** (2023), no. 1 031, [[arXiv:2212.01394](#)].
- [46] S. Chapman, D. A. Galante, E. Harris, S. U. Sheorey, and D. Vegh, *Complex geodesics in de Sitter space*, *JHEP* **03** (2023) 006, [[arXiv:2212.01398](#)].
- [47] M. Mirbabayi, *An observer’s measure of de Sitter entropy*, *JHEP* **10** (2024) 077, [[arXiv:2311.07724](#)].
- [48] S. H. Shenker and D. Stanford, *Black holes and the butterfly effect*, *JHEP* **03** (2014) 067, [[arXiv:1306.0622](#)].
- [49] L. Aalsma and G. Shiu, *Chaos and complementarity in de Sitter space*, *JHEP* **05** (2020) 152, [[arXiv:2002.01326](#)].
- [50] Y. Sekino and L. Susskind, *Fast Scramblers*, *JHEP* **10** (2008) 065, [[arXiv:0808.2096](#)].
- [51] L. Susskind, *Entanglement and Chaos in De Sitter Space Holography: An SYK Example*, *JHAP* **1** (2021), no. 1 1–22, [[arXiv:2109.14104](#)].
- [52] R. Bousso, B. Freivogel, and I.-S. Yang, *Eternal Inflation: The Inside Story*, *Phys. Rev. D* **74** (2006) 103516, [[hep-th/0606114](#)].
- [53] D. Stanford, *More quantum noise from wormholes*, [arXiv:2008.08570](#).
- [54] A. Strominger, *The dS / CFT correspondence*, *JHEP* **10** (2001) 034, [[hep-th/0106113](#)].
- [55] J. M. Maldacena, *Non-Gaussian features of primordial fluctuations in single field inflationary models*, *JHEP* **05** (2003) 013, [[astro-ph/0210603](#)].
- [56] A. A. Starobinsky, *STOCHASTIC DE SITTER (INFLATIONARY) STAGE IN THE EARLY UNIVERSE*, *Lect. Notes Phys.* **246** (1986) 107–126.
- [57] A. A. Starobinsky and J. Yokoyama, *Equilibrium state of a selfinteracting scalar field in the De Sitter background*, *Phys. Rev. D* **50** (1994) 6357–6368, [[astro-ph/9407016](#)].
- [58] G. F. Giudice, M. McCullough, and T. You, *Self-organised localisation*, *JHEP* **10** (2021) 093, [[arXiv:2105.08617](#)].
- [59] S. Jung and T. Kim, *Hubble selection of the weak scale from QCD quantum critical point*, *Phys. Rev. Res.* **4** (2022), no. 2 L022048, [[arXiv:2107.02801](#)].
- [60] J. Cotler, K. Jensen, and A. Maloney, *Low-dimensional de Sitter quantum gravity*, *JHEP* **06** (2020) 048, [[arXiv:1905.03780](#)].
- [61] F. Loran, *Massive spinors and dS/CFT correspondence*, *JHEP* **06** (2004) 054, [[hep-th/0404135](#)].
- [62] J. Jiang, *Scalar and Spinor Effective Actions in Global de Sitter*, *JHEP* **06** (2020) 037, [[arXiv:2004.06251](#)].